Nanomanufacturing
University of Michigan
ME599-002 | Winter 2010

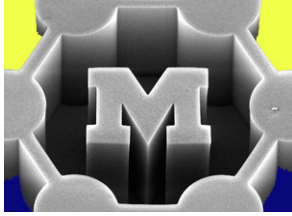

20: **From 2D to 3D – layer-by-layer assembly and colloidal crystals**

April 5, 2010

John Hart
ajohnh@umich.edu
http://www.umich.edu/~ajohnh

Announcements

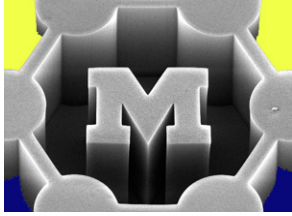

- Did I meet with all the project teams?
- No lecture Wednesday
- PS4 due next Monday (Apr/12)

- EXAM
  - Mean = 57/100
  - Stdev = 13
  - High = 84

- PS3
  - Mean = 3.2/4
  - Stdev = 0.5
  - High = 4

Upcoming lectures

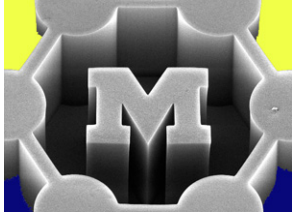

- M Apr/12
  - Self-assembly using external forces
- W Apr/14
  - Joining nanostructures and network properties
- Extra (slides only)
  - Nanocomposites and yarns

Recap: self-assembled monolayers (SAMs)

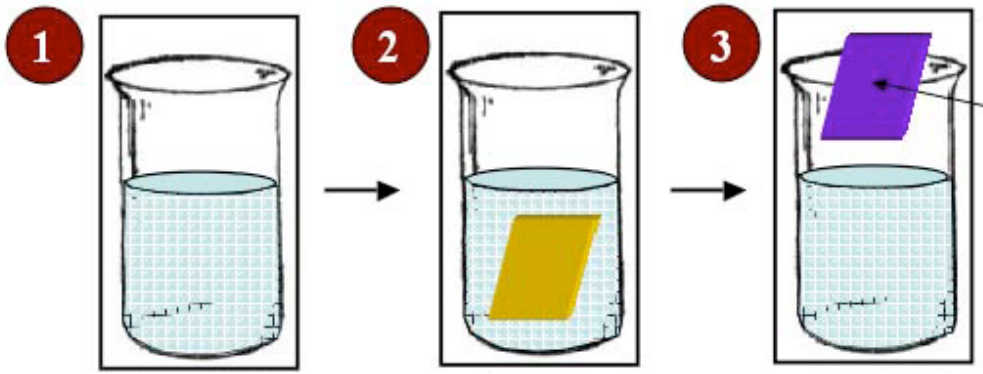

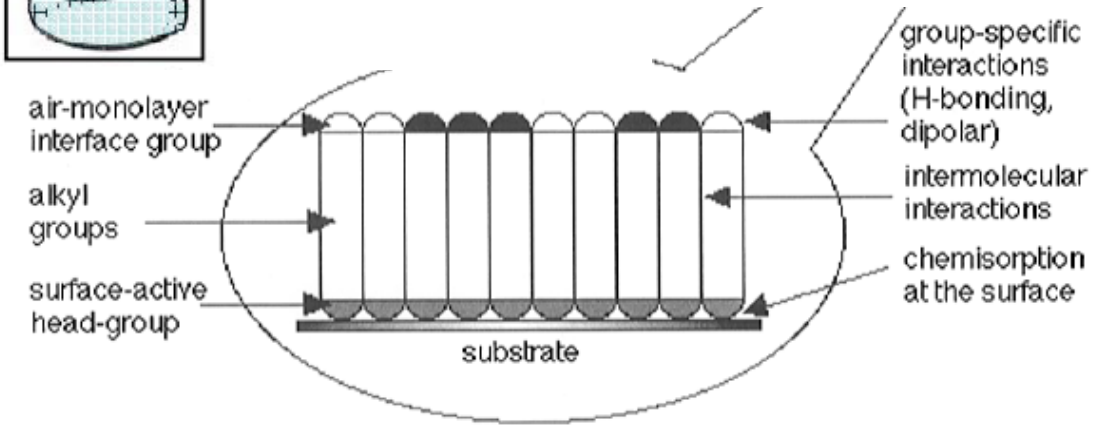

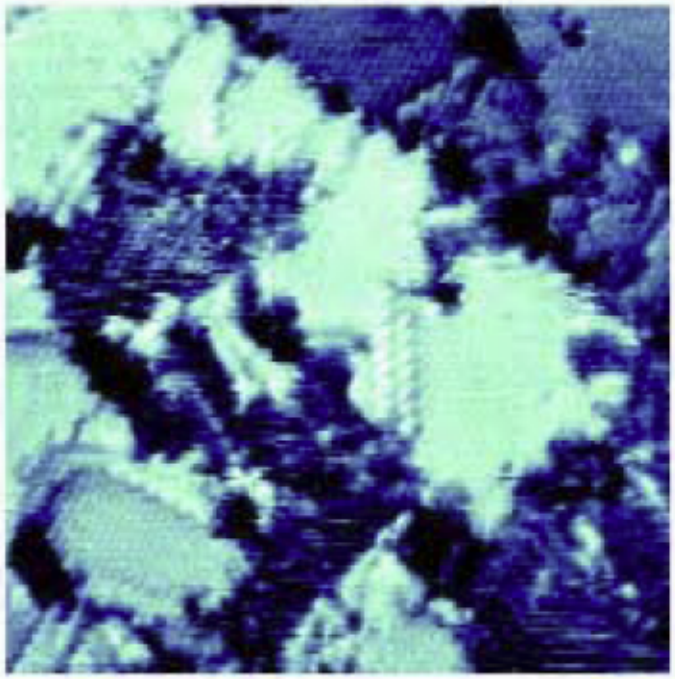

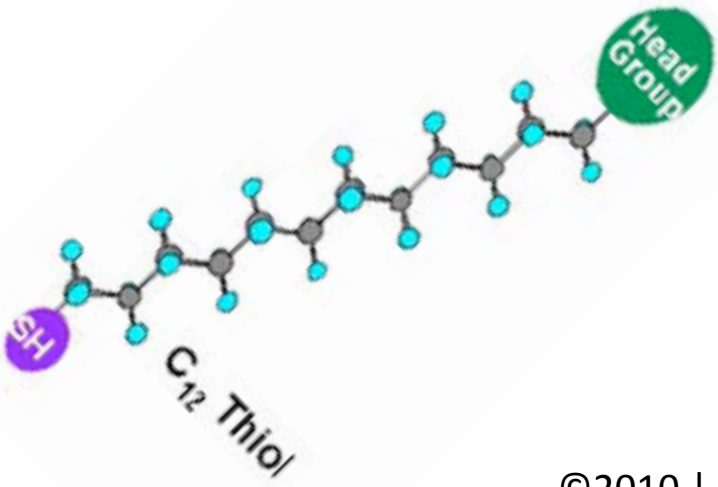

Self-stratified SAMs on Au nanoparticles

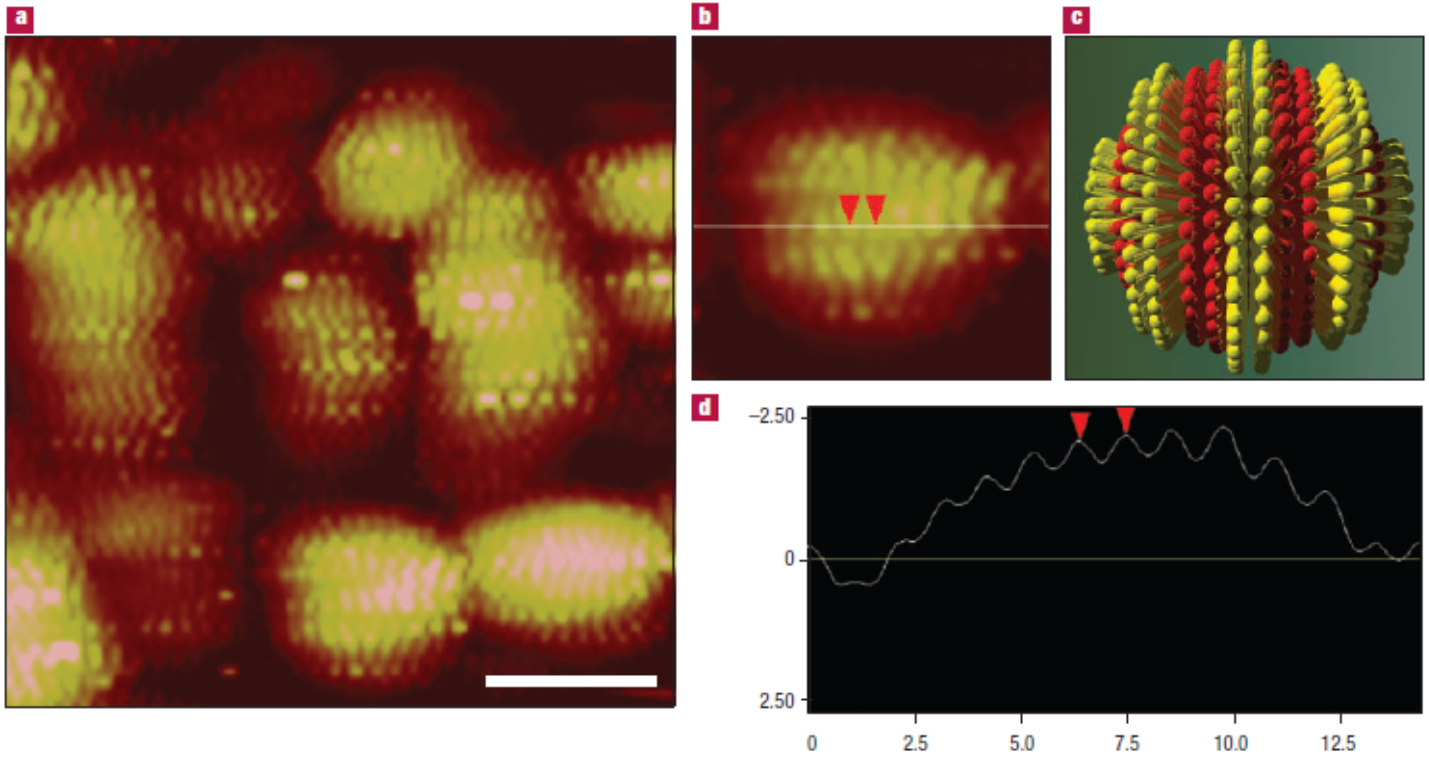

OT = octanethiol, CH_3-$(CH_2)_7$-SH; and
MPA = mercaptopropionic acid, HOOC-$(CH_2)_2$-SH
→ Note thiol (S) end groups

Jackson, Myerson, Stellacci, *Nature Materials.* 3:1-7, 2004.

Domain organization determined by entropy and substrate curvature

Increasing chain length difference

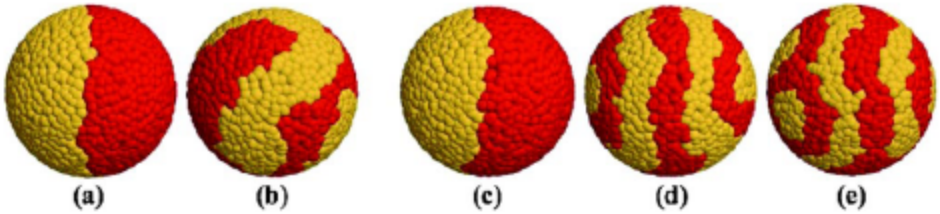

FIG. 3 (color online). Equilibrium structures obtained by mesoscale simulations of self-assembly of binary mixtures of surfactants with varying length difference or bulkiness difference on a sphere of radius 5σ. Dark (red) beads and light (yellow) beads represent head groups of the two species of surfactants (tails not shown). (a) Length ratio 4:4, equal bulkiness. (b) Length ratio 6:6 with one surfactant (yellow heads) having a bulkier tail group. (c)–(e) Length ratios 4:6, 4:7 and 4:13, respectively, with equal bulkiness.

- Chain length difference = chains want more room to maximize entropy
- Smaller particle = more room due to curvature

Increasing particle diameter

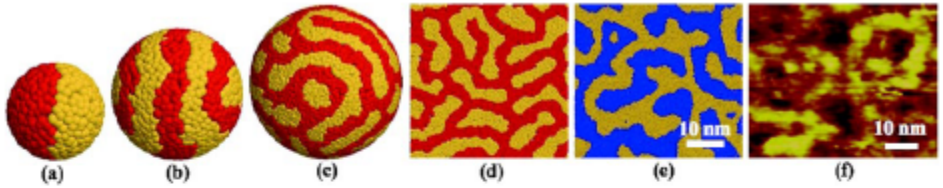

FIG. 4 (color online). (a)–(d) Equilibrium structures obtained by mesoscale simulations of self-assembly of a binary mixture of surfactants of length ratio 4:7 on surfaces with varying degrees of curvature. Dark (red) beads and light (yellow) beads represent

Singh et al., *Phys. Rev Lett.* 99:226106, 2007.

Recap: the Langmuir-Blodgett method

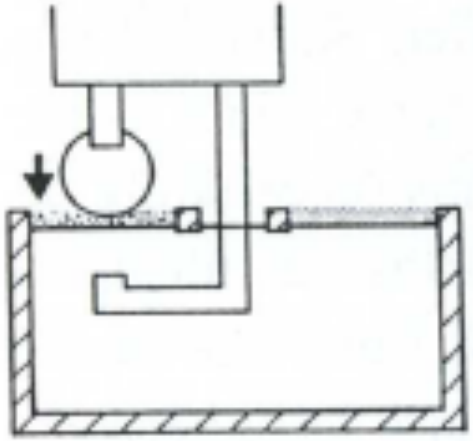

Step 1

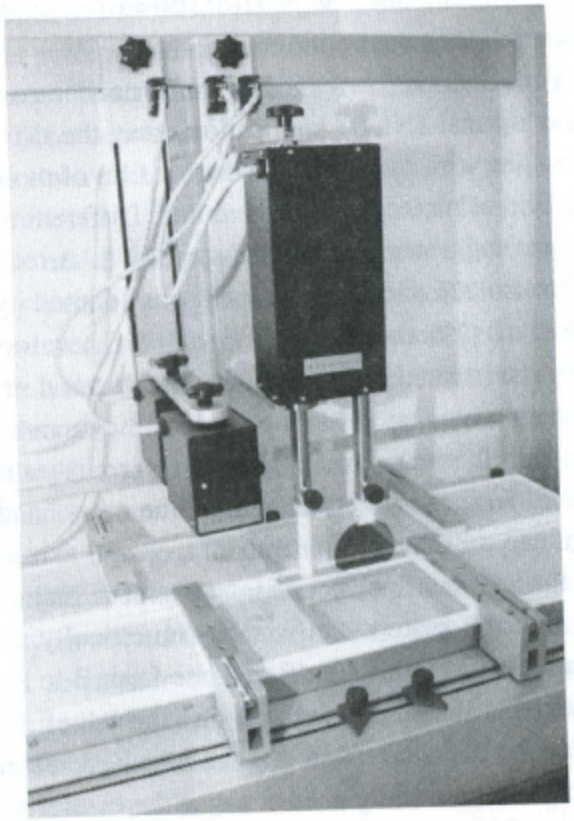

Figure 2.2. The KSV 5000 trough.

LB of Ag nanowires (like logging)

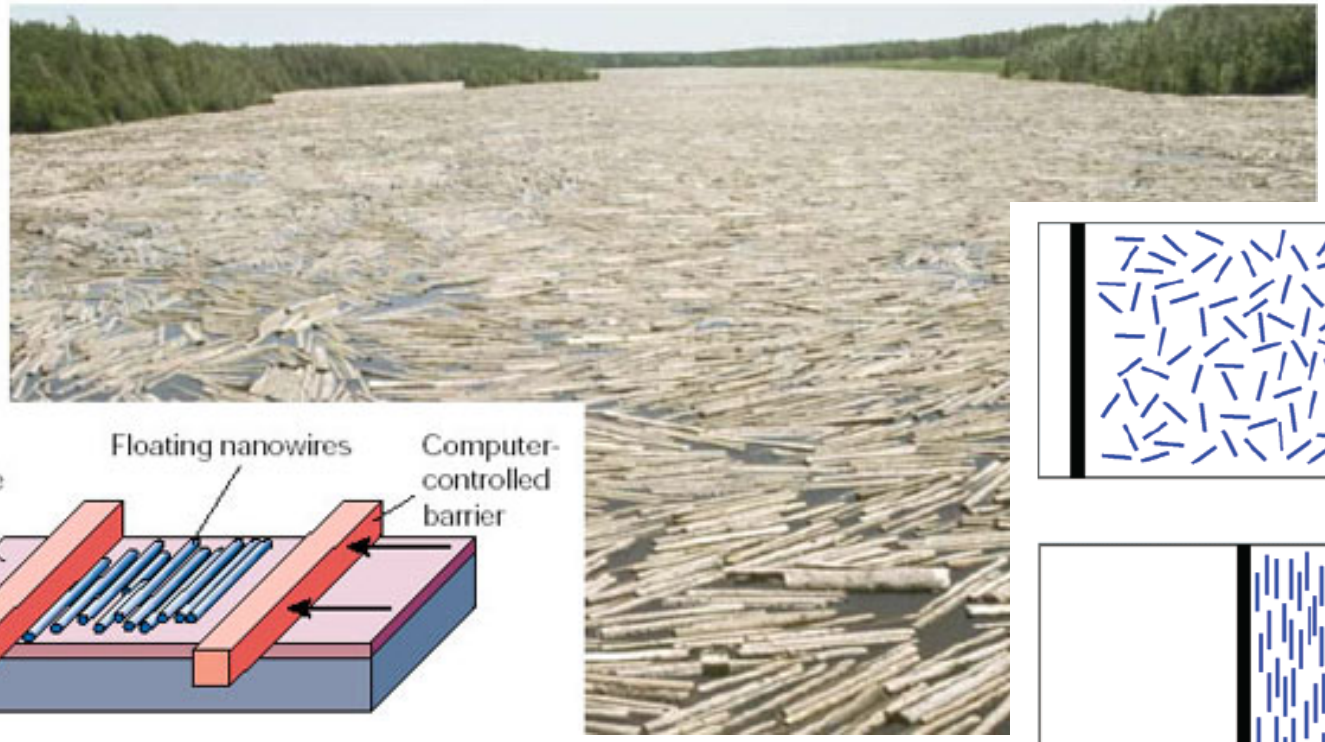

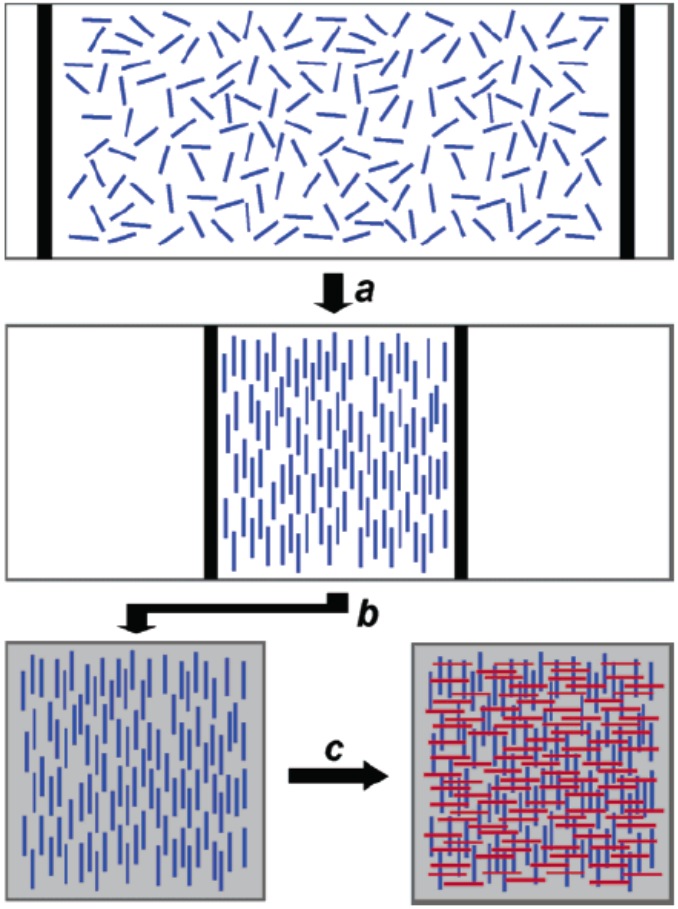

Tao et al., *Nano Lett.* 3(9):1229, 2003.
Whang et al., *Nano Lett.* 3(9):1255, 2003

Surface pressure increases as monolayer is compacted

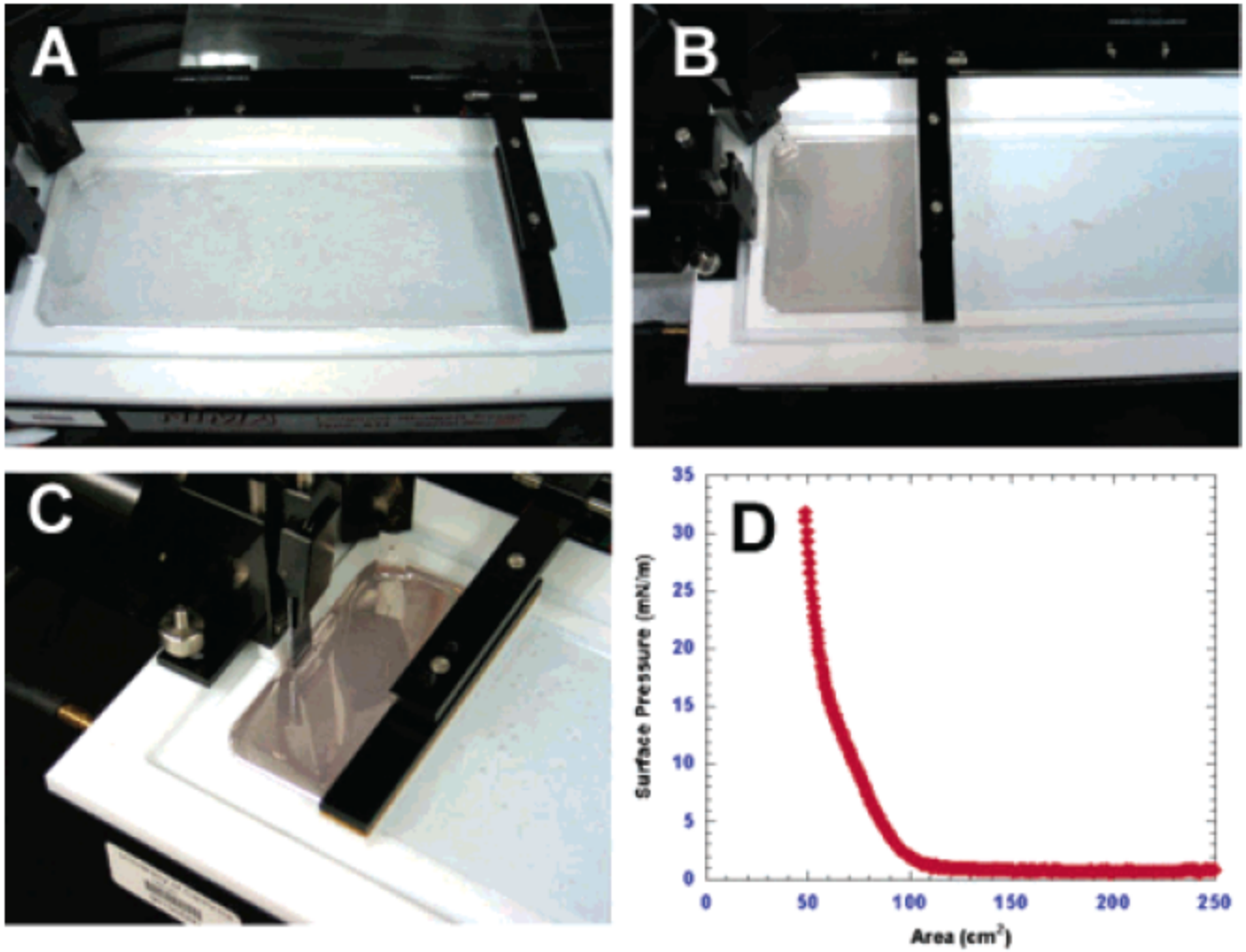

Tao et al., *Nano Lett.* 3(9):1229, 2003.

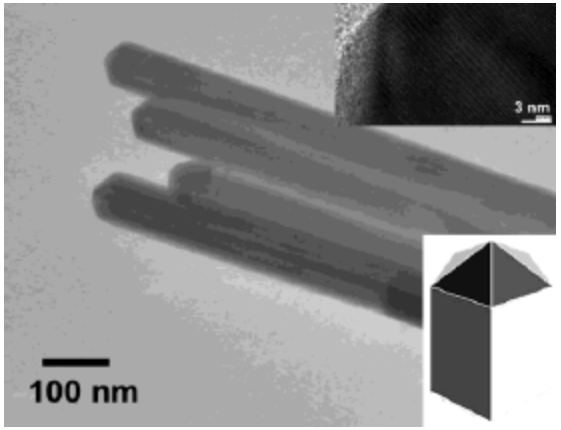

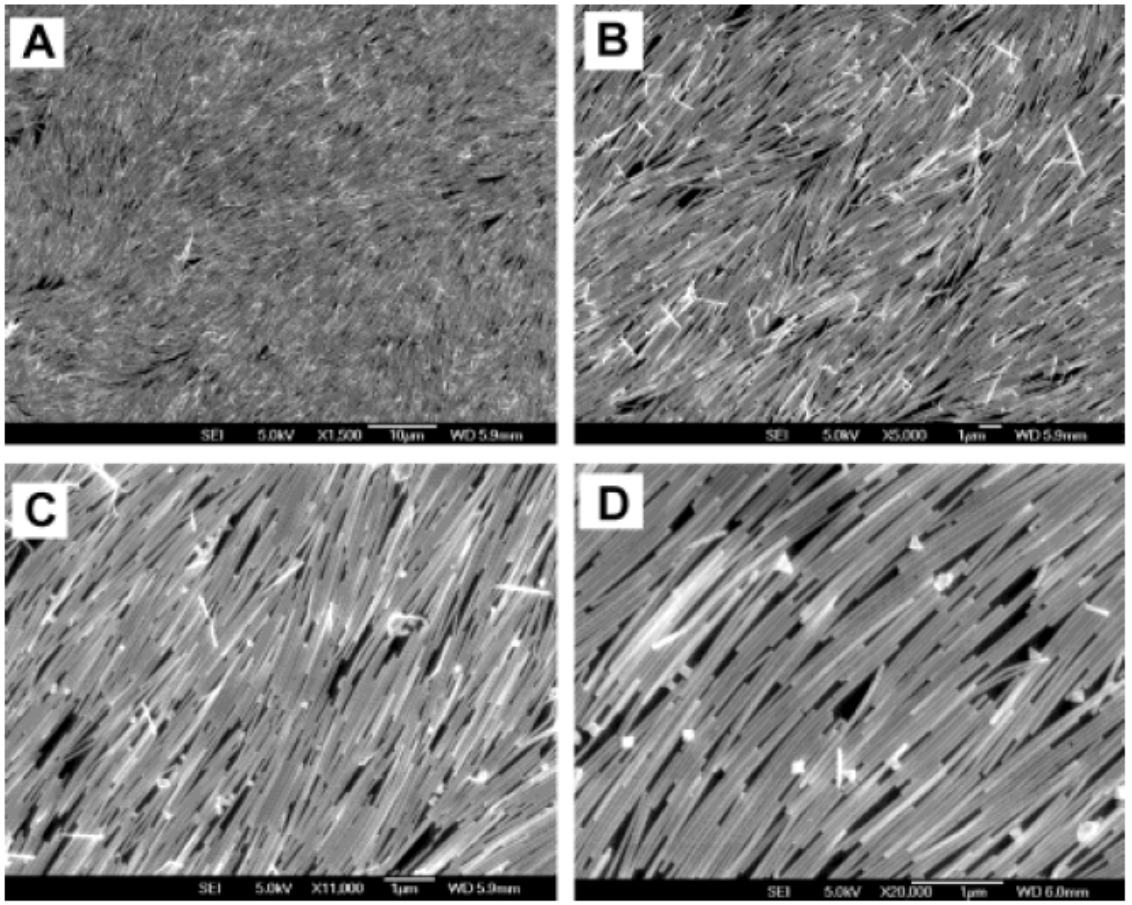

Figure 3. Scanning electron microscopy images (at different magnifications) of the silver nanowire monolayer deposited on a silicon wafer.

Tao et al., *Nano Lett.* 3(9):1229, 2003.

LB deposition of graphene (oxide) films

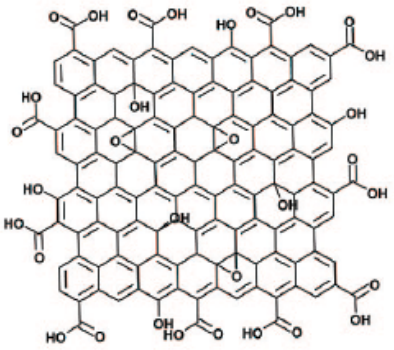

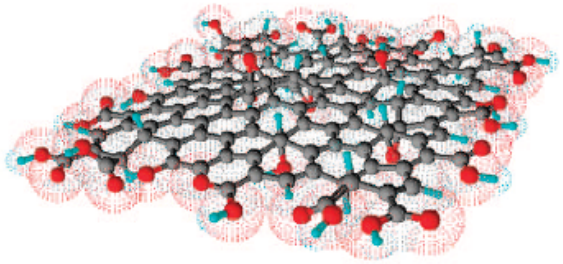

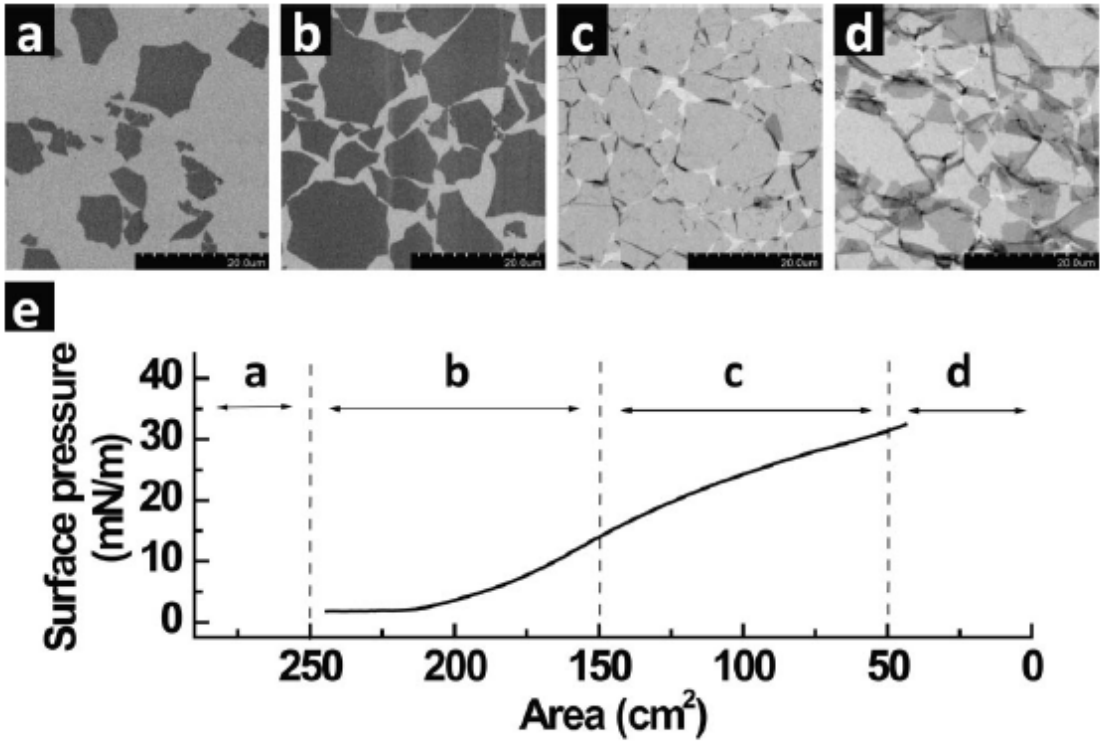

Figure 2. Langmuir−Blodgett assembly of graphite oxide single layers. (a−d) SEM images showing the collected graphite oxide monolayers on a silicon wafer at different regions of the isotherm. The packing density was continuously tuned: (a) dilute monolayer of isolated flat sheets, (b) monolayer of close-packed GO, (c) overpacked monolayer with sheets folded at interconnecting edges, and (d) over packed monolayer with folded and partially overlapped sheets interlocking with each other. (e) Isothermal surface pressure/area plot showing the corresponding regions a−d at which the monolayers were collected. Scale bars in a-d represent 20 μm.

Cote et al., JACS 131:1043-1049, 2009.

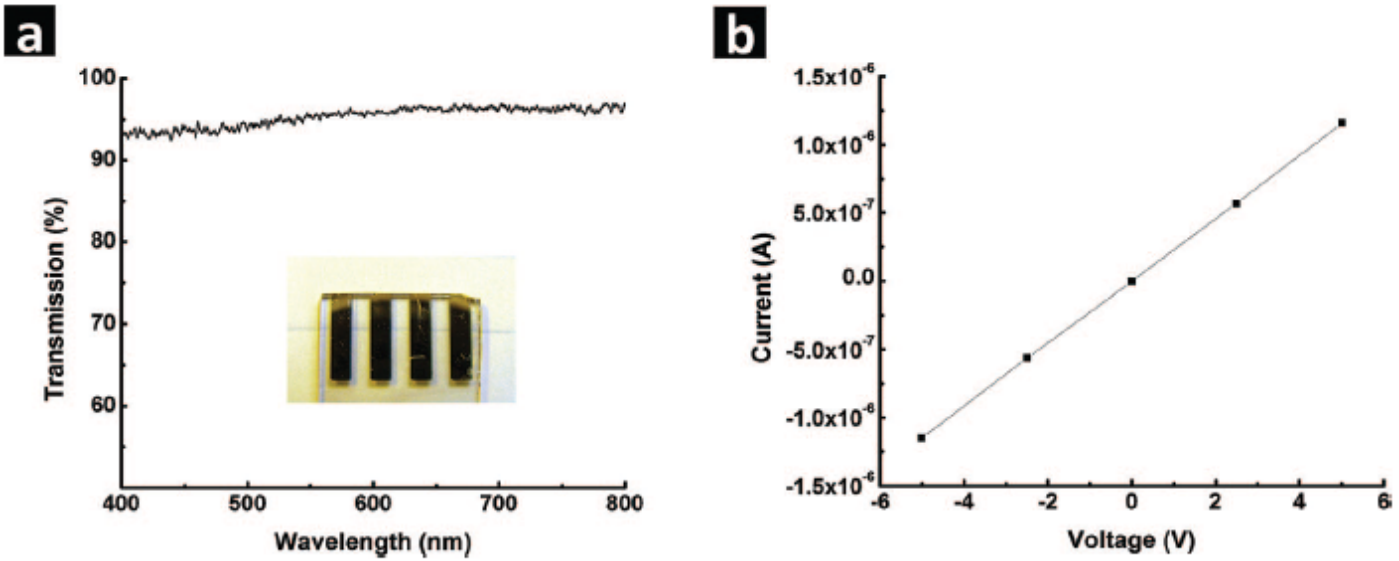

Figure 6. Transparent conducting thin film obtained by chemical reduction of an overpacked, interlocking GOSL monolayer such as those collected from region d of the isotherm plot in Figure 2. (a) Transmission spectrum of such a thin film deposited on a glass slide (inset), showing an average of 95.4% transmittance in the visible region. (b) Current−voltage plot of the same film obtained by four-point measurement.

From synthesis to assembly

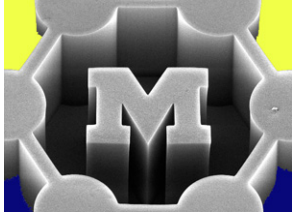

2D

- Film deposition and growth (physical/chemical):
  - growth of films of nanotubes/wires
  - monolayer self-assembly

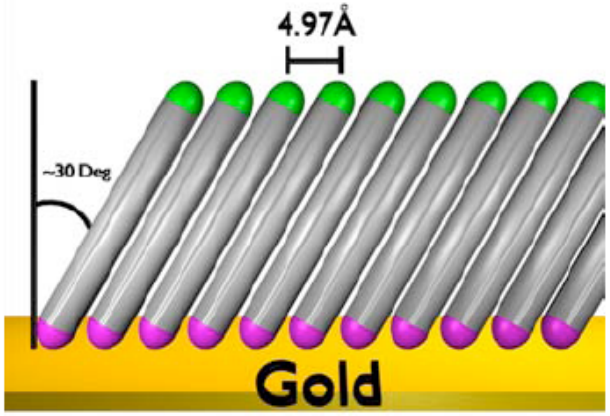

3D (all effects together)

- Colloidal crystals, superlattices
- Yarn spinning, networks, aerogels, composites, etc.

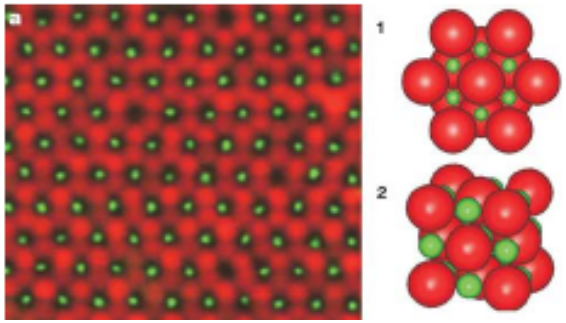

The goal is to maintain order as we scale up!

Today's agenda

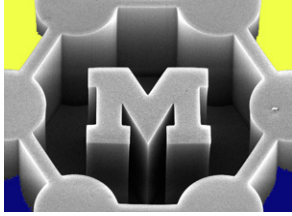

- Layer-by-layer (LBL) assembly
- Packing of micro- and nanoparticles into "colloidal crystals" using capillary forces

Today's readings

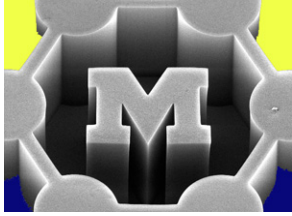

Nominal: (ctools)

- Decher, "Fuzzy nanoassemblies: toward layered polymeric multicomposites"
- Krogman et al., "Spraying asymmetry into functional membranes layer-by-layer"
- Chen et al., "Evaporation-induced assembly of quantum dots into nanorings"

Extras: (ctools)

- Podsiadlo et al., "Ultrastrong and stiff layered polymer nanocomposites"
- Rycenga et al., "Template-assisted self-assembly: a versatile approach to complex micro- and nanostructures"

Layer-by-layer (LBL) assembly

Form stacked nanolayers by sequential adsorption of oppositely charged species (e.g., polymers, nanoparticles)

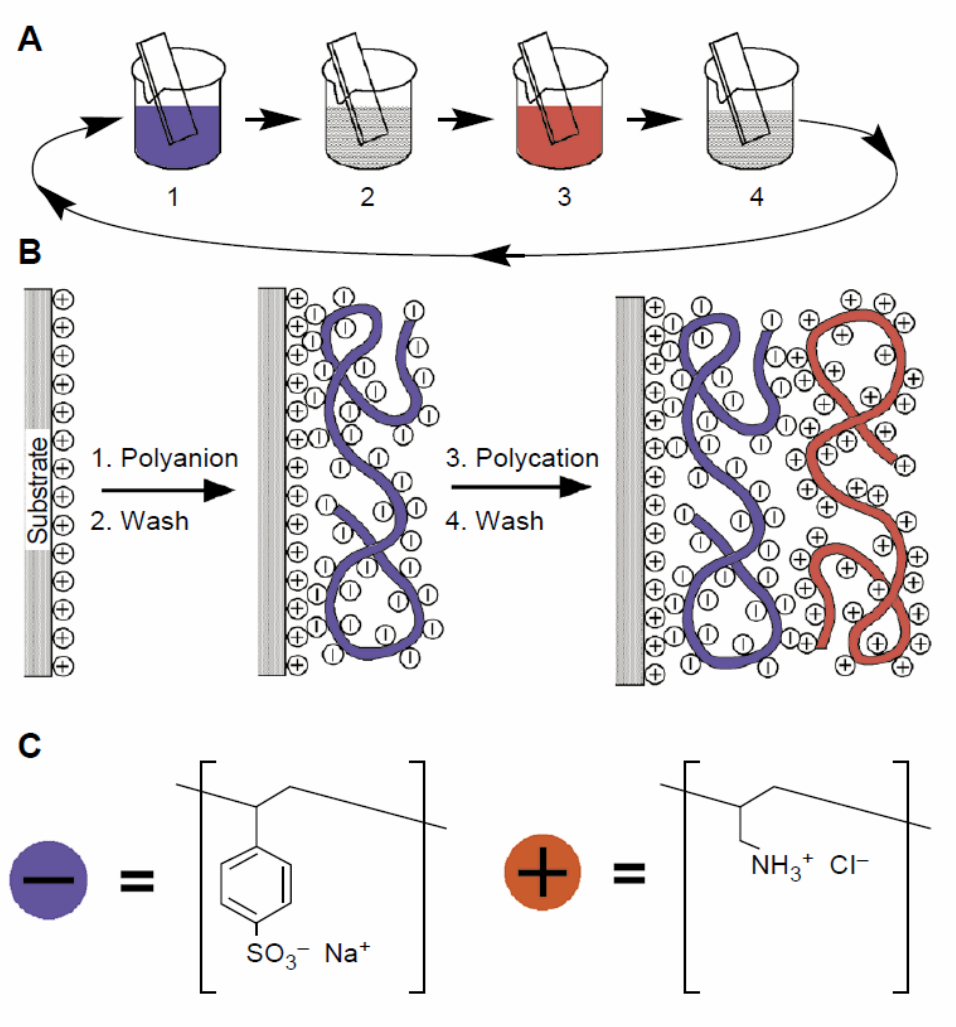

"Fuzzy" layers, nanometers thick

Extends versatility beyond SAM and LB

Dip, spray, roll, …

Decher, *Science* 277:1232-7, 1997.

Layer design

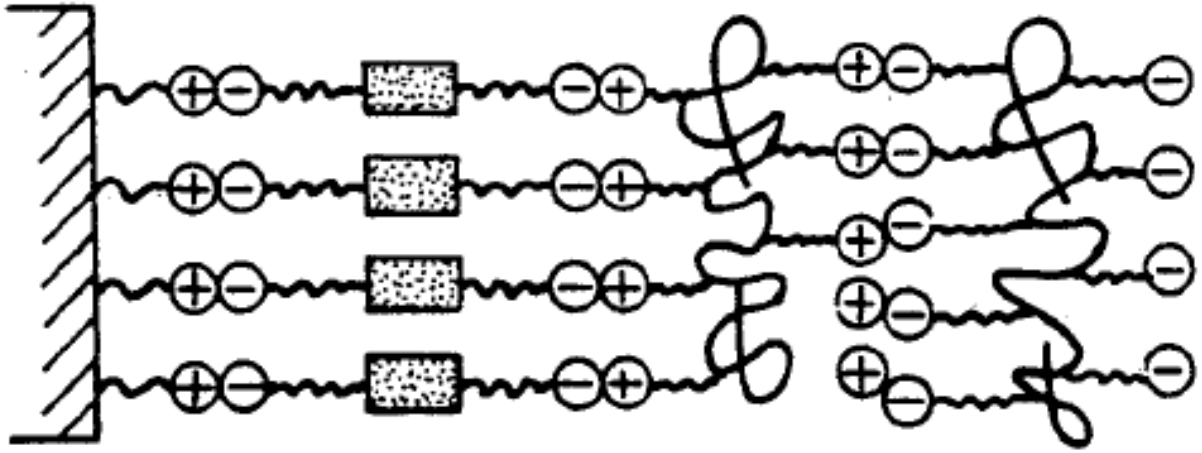

Decher et al.

Oscillation of surface (zeta) potential

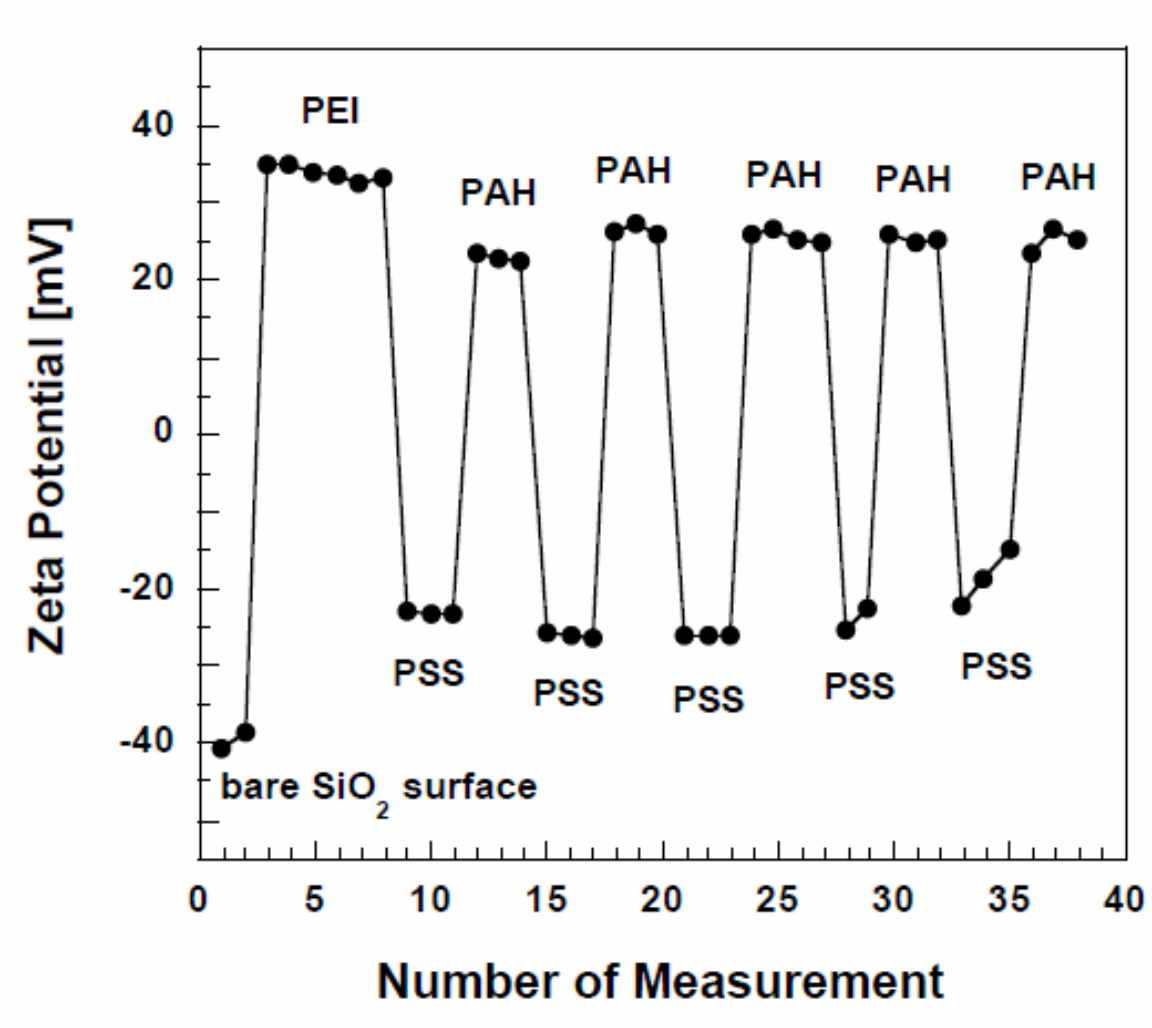

Decher.

Interdiffusion of layers

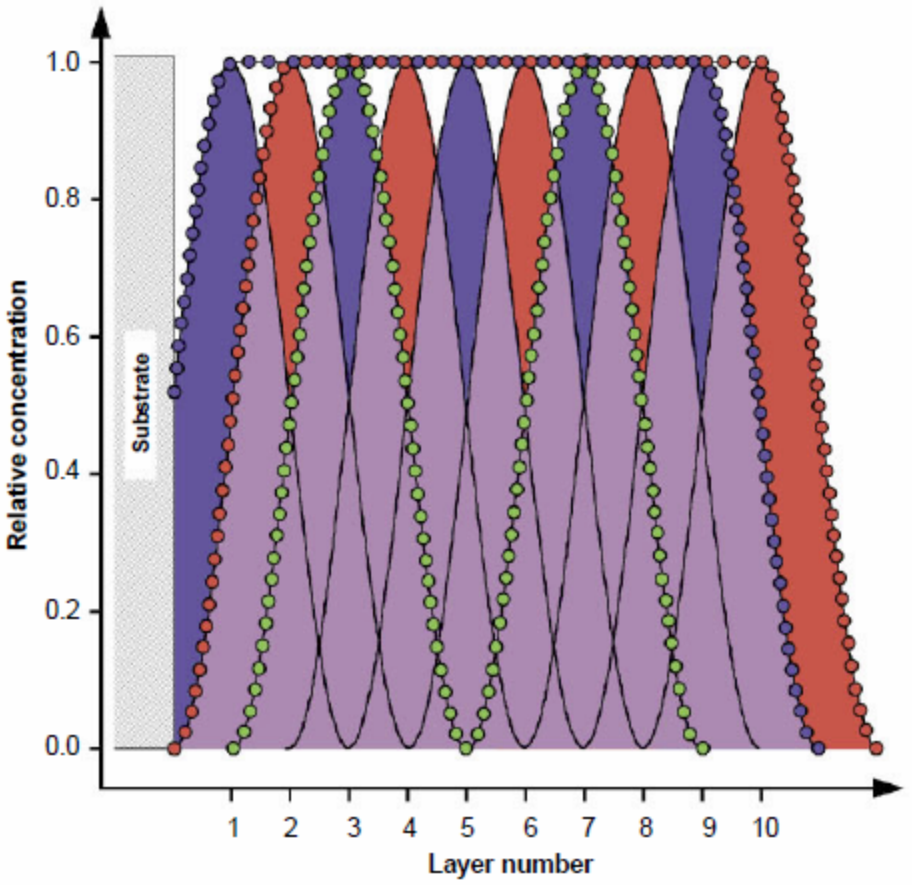

Fig. 3. Schematic of a polyelectrolyte multilayer composed of 10 layers, each represented by an arbitrarily chosen sinusoidal concentration profile (black lines). For a positively charged substrate, the five blue layers and five red layers represent polyanion and polycation layers, respectively. The spread of each layer and the distance between them were chosen such that every two layers of equal charge start to overlap at a relative concentration of 50%. The overlap of blue and red layers (purple) has no physical meaning. The lines composed of blue dots (anionic groups) and red dots (cationic groups) represent the sum of concentrations from all layers within the film. A positional shift of red layers with respect to blue layers causes changes in charge concentration only at the two interfaces, not in the center of the film. The line composed of green dots represents the concentration profile for a label applied to every fourth layer $[(A/B/A/B_d)_n$ architecture = deuterium labels in layers 3 and 7].

Decher, *Science* 277:1232-7, 1997.

LBL can involve nearly any type of macromolecule

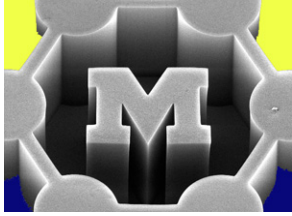

- Nanoparticles, nanotubes, nanowires
- Nanoplatelets (e.g., clay)
- Dyes
- Dendrimers
- DNA, proteins, viruses
- etc…

To make

- Composites, membranes
- Antireflective, superhydrophobic surfaces
- Controlled-desorption (e.g., drug delivery) or anti-absorption (e.g., antibacterial) coatings
- Solar cells, batteries
- etc…

Lab-scale LBL “robot”

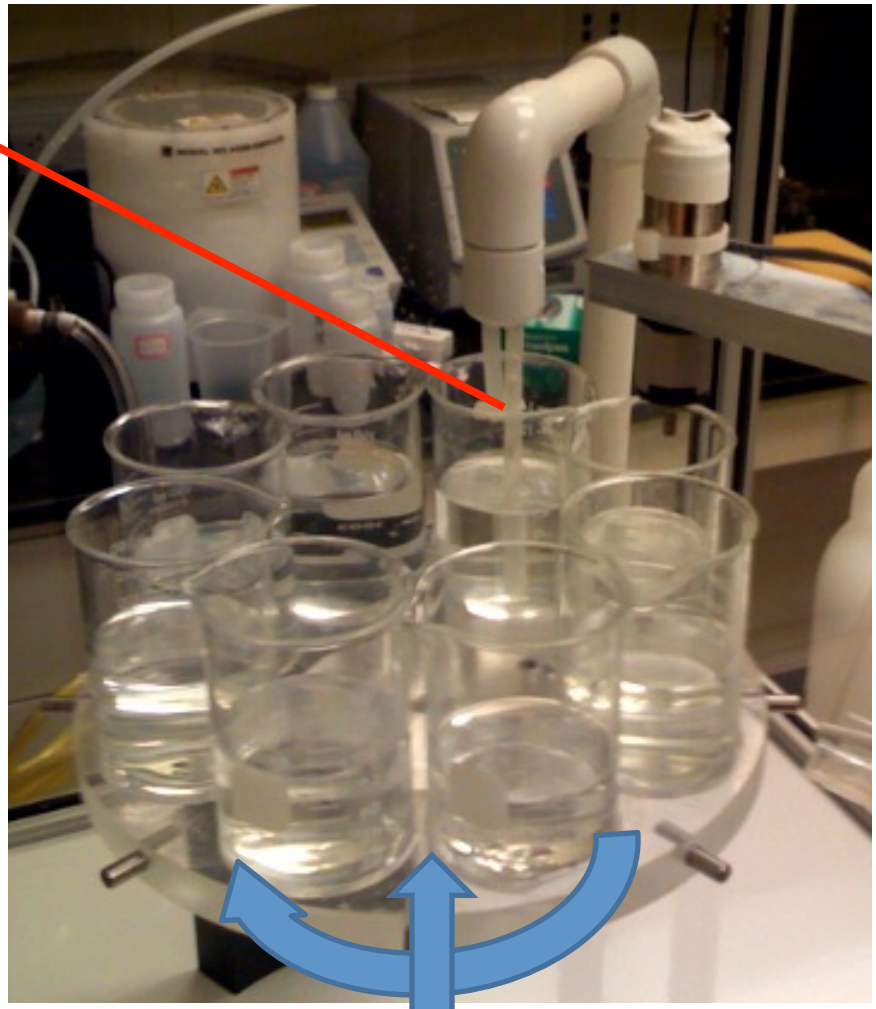

Polymer-clay nanocomposites by LBL

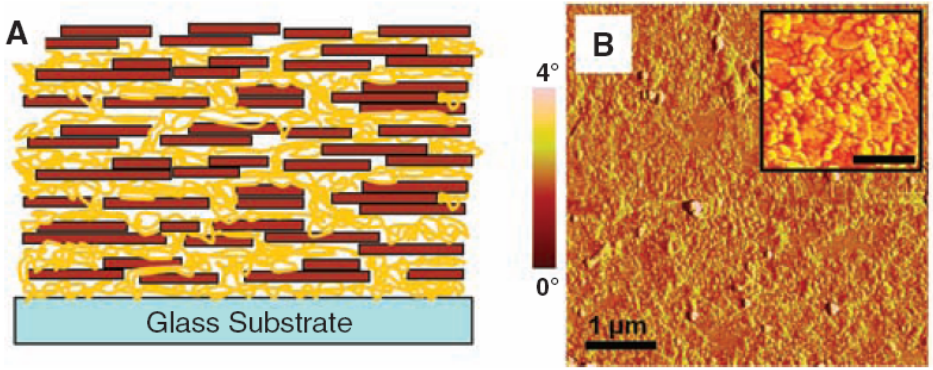

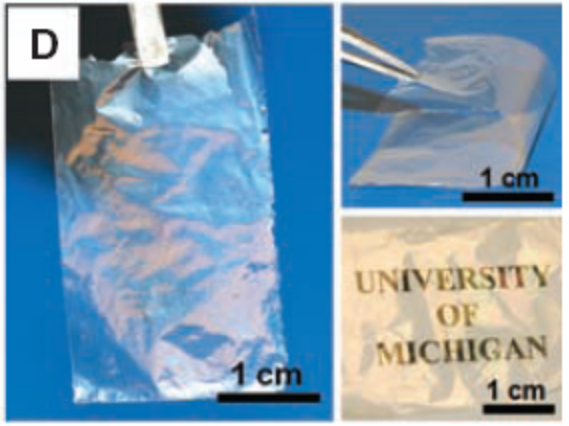

Fig. 1. Preparation of PVA/MTM nanocomposites. (**A**) Schematic representation of the internal architecture of the PVA/MTM nanocomposite (picture shows 8 bilayers). (**B**) ATM phase image of a single PVA/MTM bilayer adsorbed on top of a silicon wafer. (Inset) Close up of the main image showing individual MTM platelets more clearly. Scale bar in inset, 400 nm. (**C**)

Fig. 2. Scanning electron microscopy characterization of a 300-bilayer, free-standing PVA/MTM nanocomposite. (**A**) Cross section of the film. Arrows indicate the span of the cross section. (**B**) Close-up of the cross section showing the separation of layers. (**C**) Top-down view of a fracture edge of the composite after tensile testing. Dashed line indicates edge of the sample. (**D**) Top-down view of the composite's surface. The slight separation of the layers seen in (A) and (B) is due to a shearing force resulting from cutting the sample with a razor blade during scanning electron microscopy sample preparation.

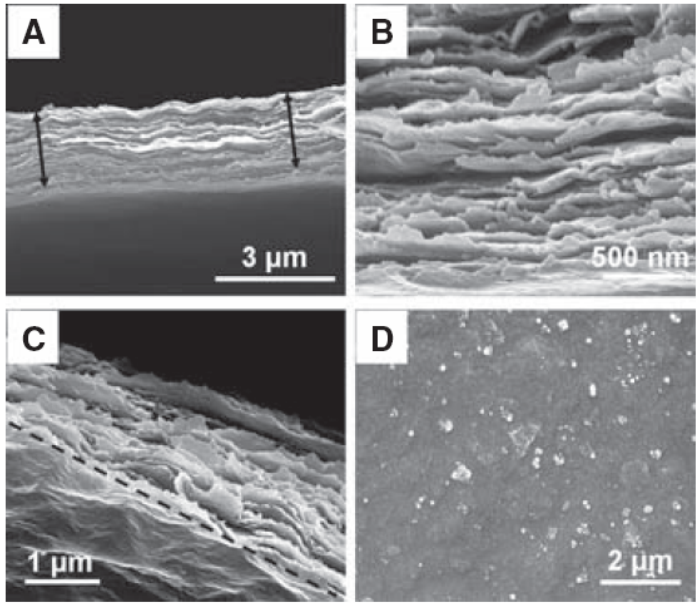

Podsiadlo et al., *Science* 318:83, 2007.

PVA (polymer)

covalent to

MTM (clay)

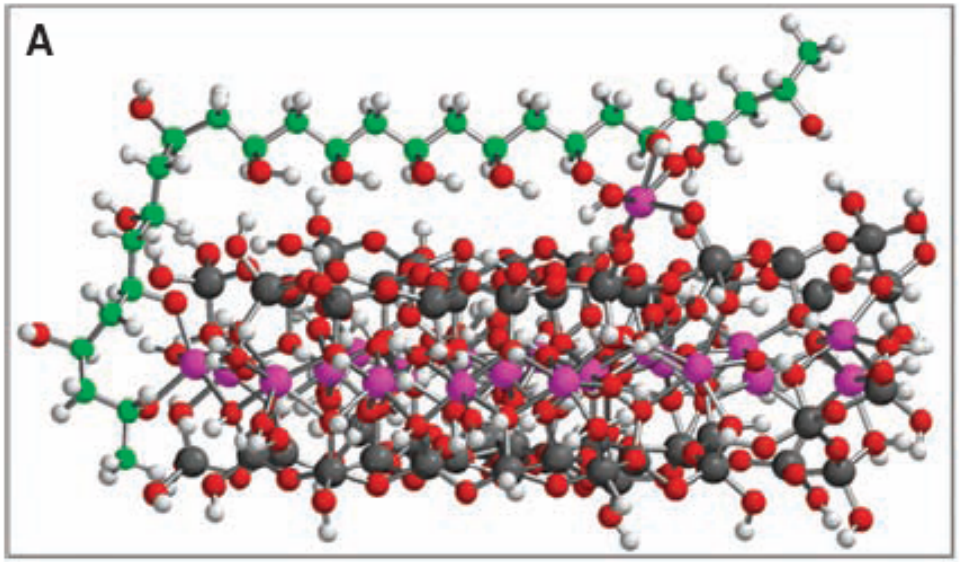

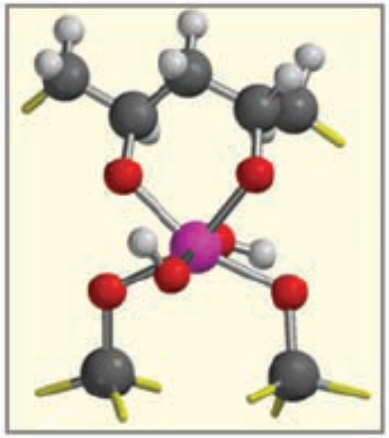

Podsiadlo et al., *Science* 318:83 2007.

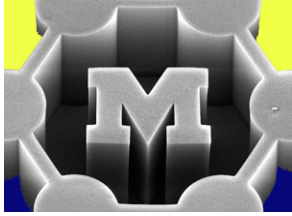

MTM/PVA

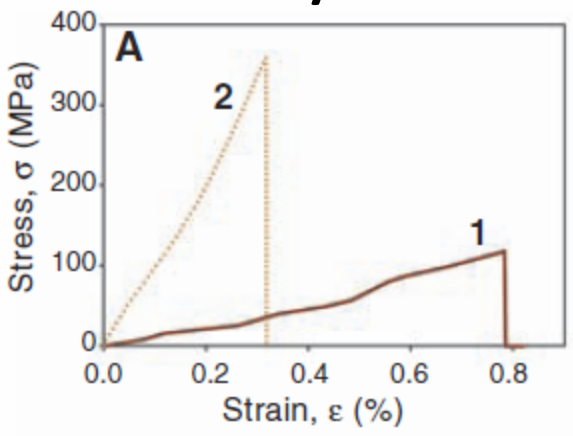

PVA

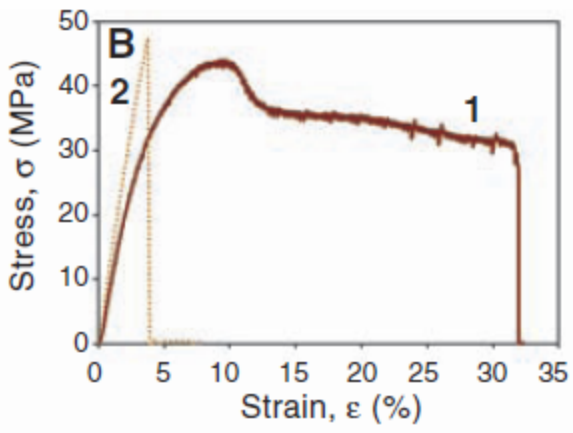

1 = no GA; 2 = GA (crosslinking)

Sample type (*N*)	Tensile strength σ_{UTS} (MPa)	Modulus *E'* (GPa)	Ultimate strain ε (%)
PVA (5)	40 ± 4	1.7 ± 0.2	35 ± 4
PVA with GA (5)	40 ± 10	2.0 ± 0.5	3.3 ± 1.3
PDDA (5)	12 ± 4	0.2 ± 0.03	48 ± 9
PDDA-MTM (*)	100 ± 10	11 ± 2	10 ± 2
PVA/MTM (5)	150 ± 40	13 ± 2	0.7 ± 0.2
PVA/MTM with GA (5)	400 ± 40	106 ± 11	0.33 ± 0.04

*Data are the previously published results by Tang *et al.* (*15*) for 1.2-to-4.9–μm–thick (50 to 200 bilayers) samples tested at relative humidity of 32%.

GA = glutyaldrehyde

Podsiadlo et al., *Science* 318:83 2007.

LBL film growth kinetics

Kinetics driven by adsorption on surface and diffusion through previously deposited layers

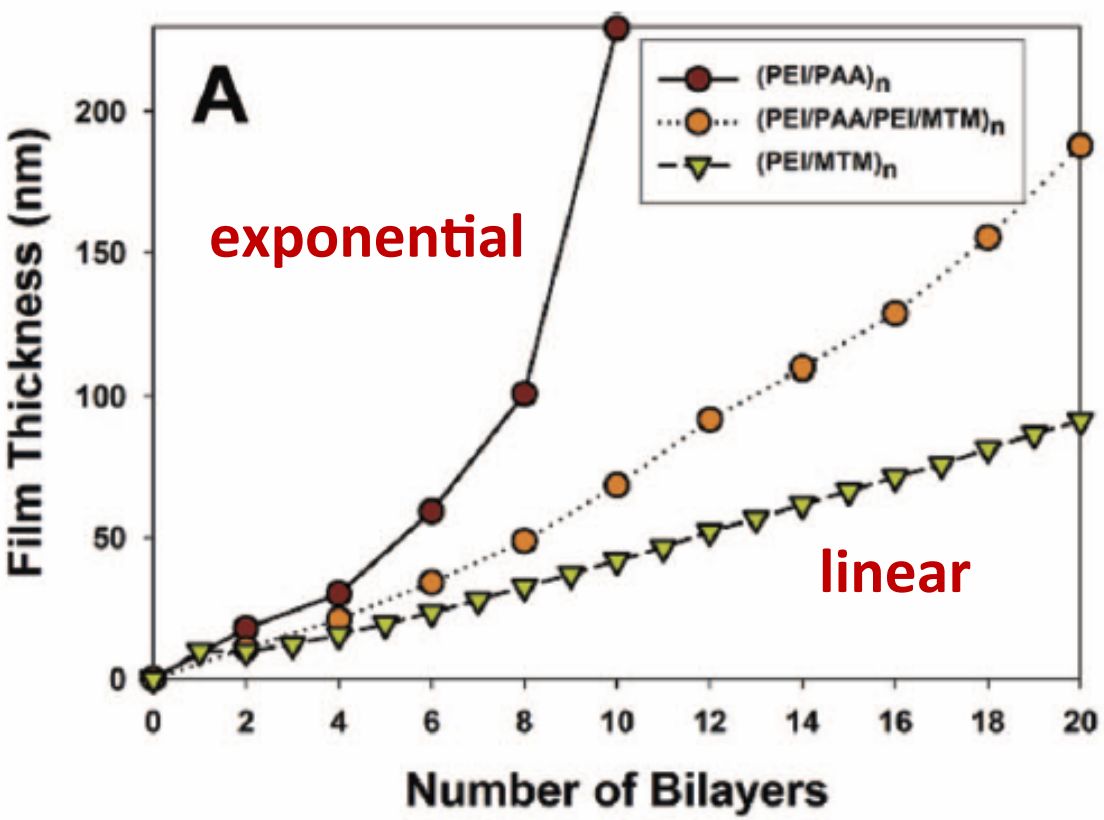

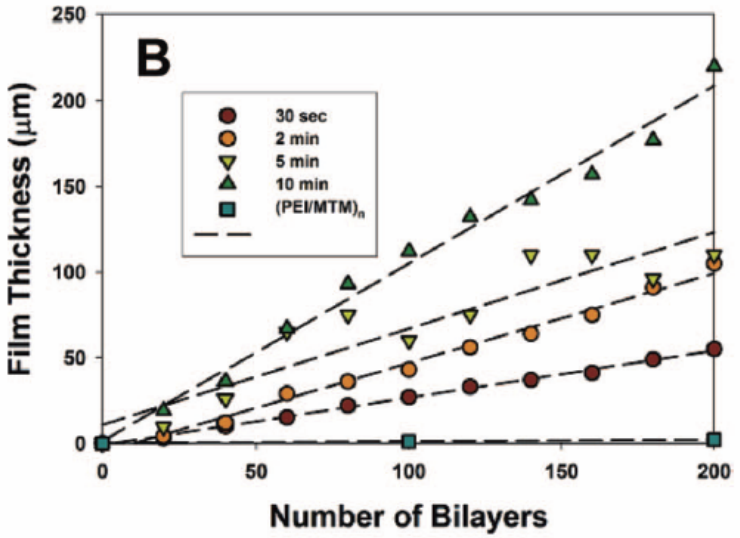

Podsiadlo et al., *Nano Letters* 8(6):1762-1770, 2008.

Spray LBL on fibers

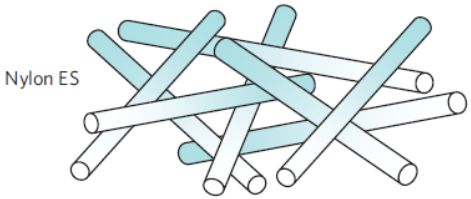

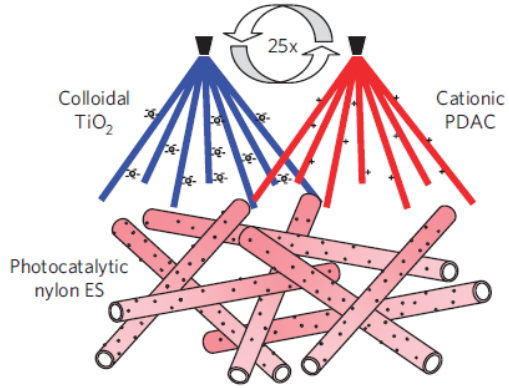

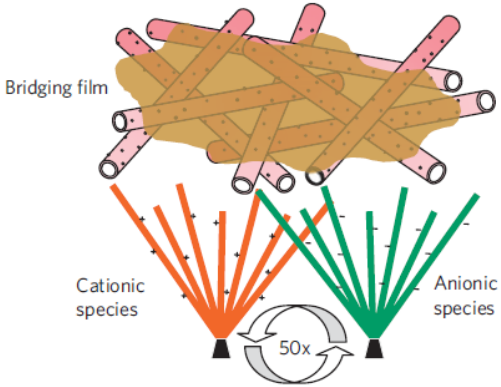

Top view

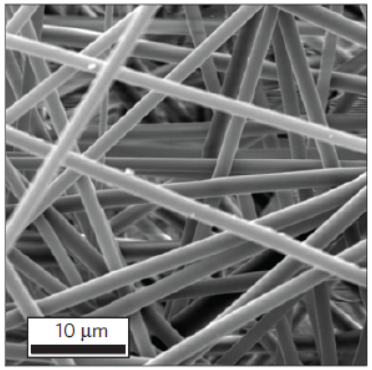

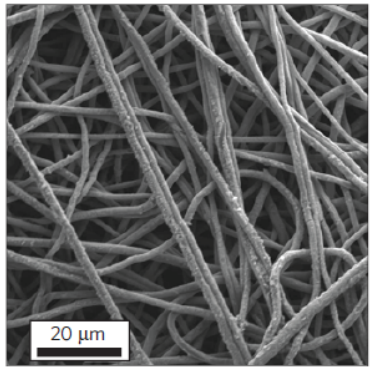

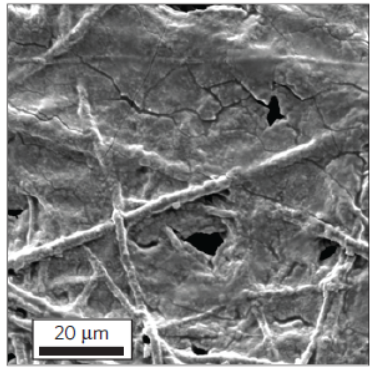

Section view

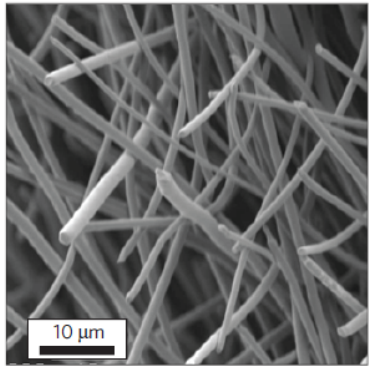

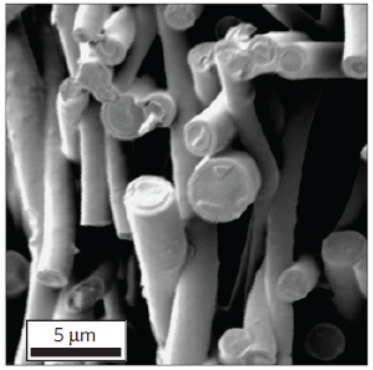

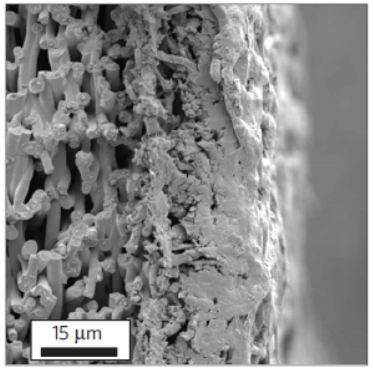

Electrospinning

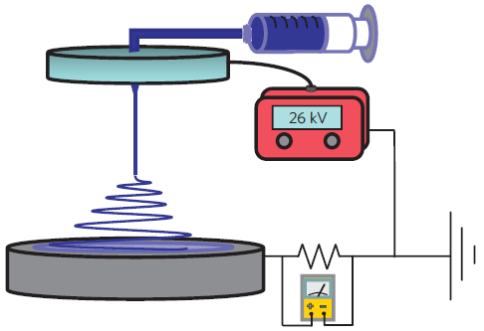

Krogman et al., *Nature Materials* 8:512-518, 2009.

Spray LBL on fibers

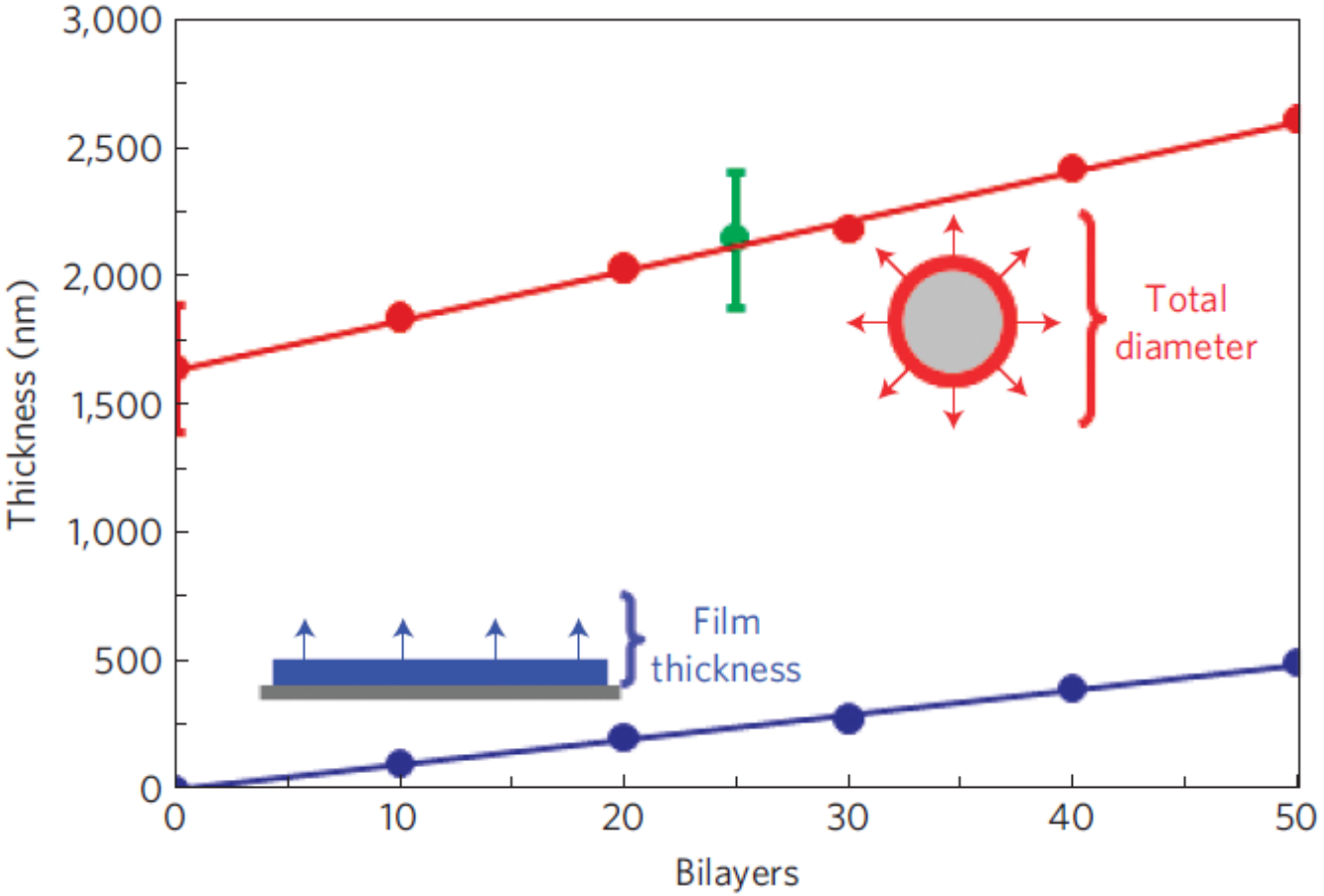

Krogman et al., *Nature Materials* 8:512-518, 2009.

Conformal vs. separated coatings

Re_D = 6.5

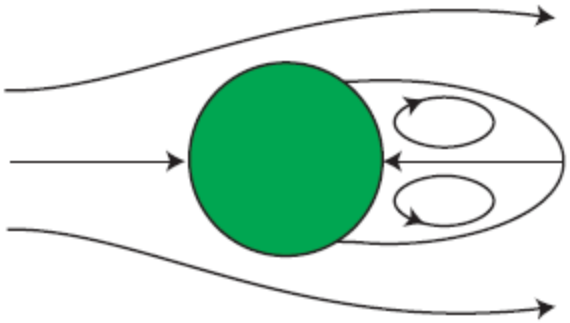

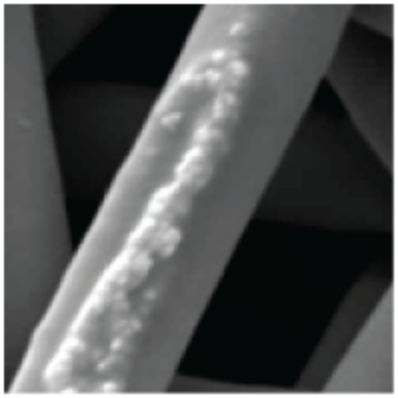

transition at Re_D ≈6

Re_D = 1.7

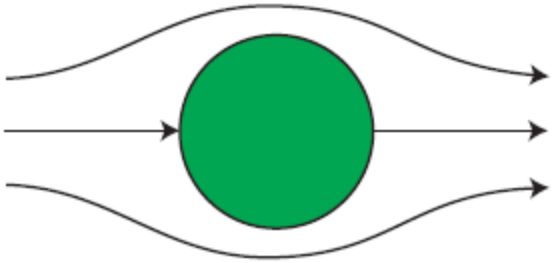

Re for a packed bed: V_S = superficial velocity, ν = viscosity, ε = void fraction of mat

$$\mathrm{Re}_D = {DV_S}/{\upsilon(1-\varepsilon)}$$

Krogman et al., *Nature Materials* 8:512-518, 2009.

LBL on spheres

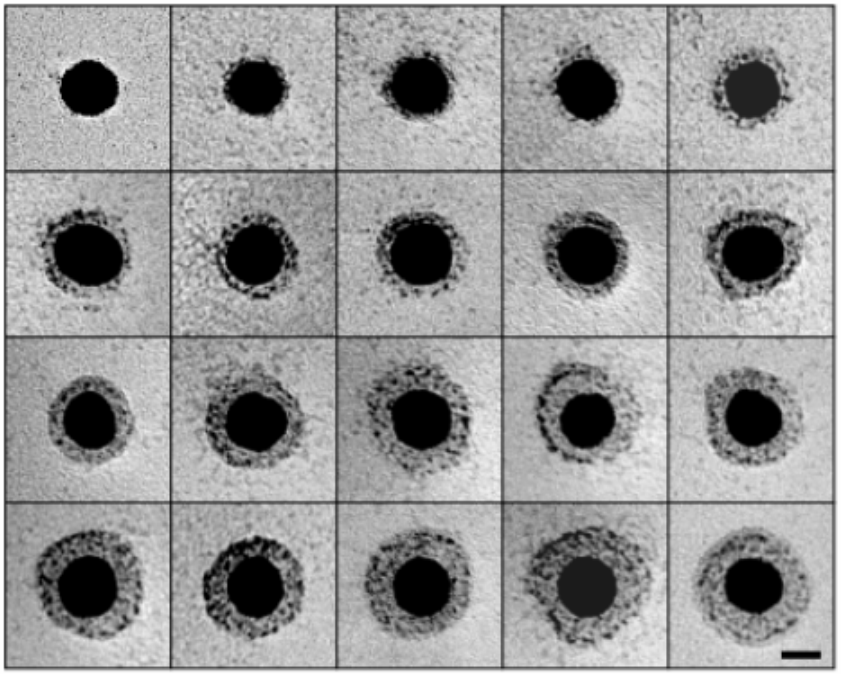

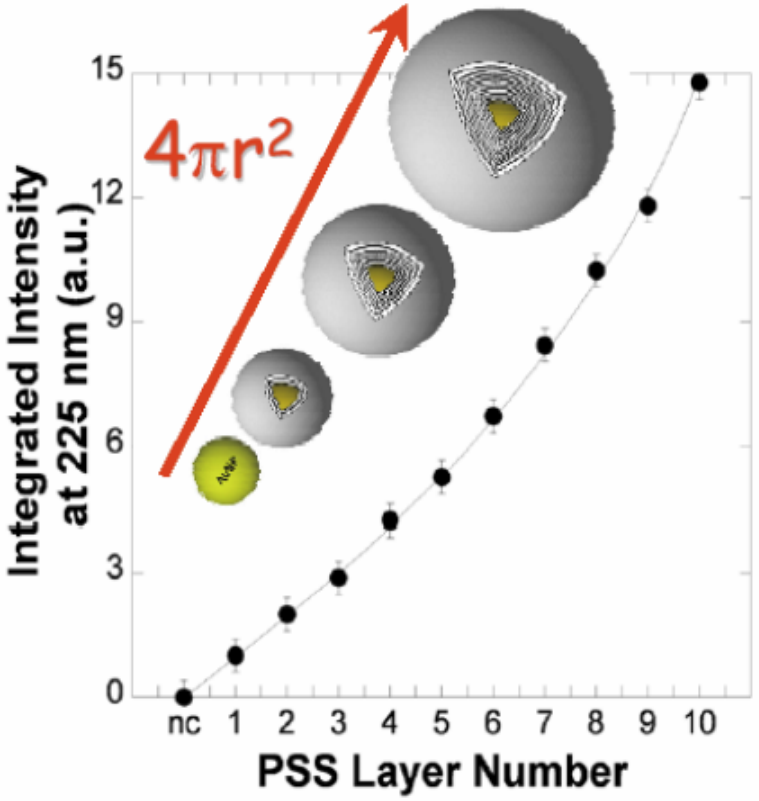

Decher.

Hollow spheres

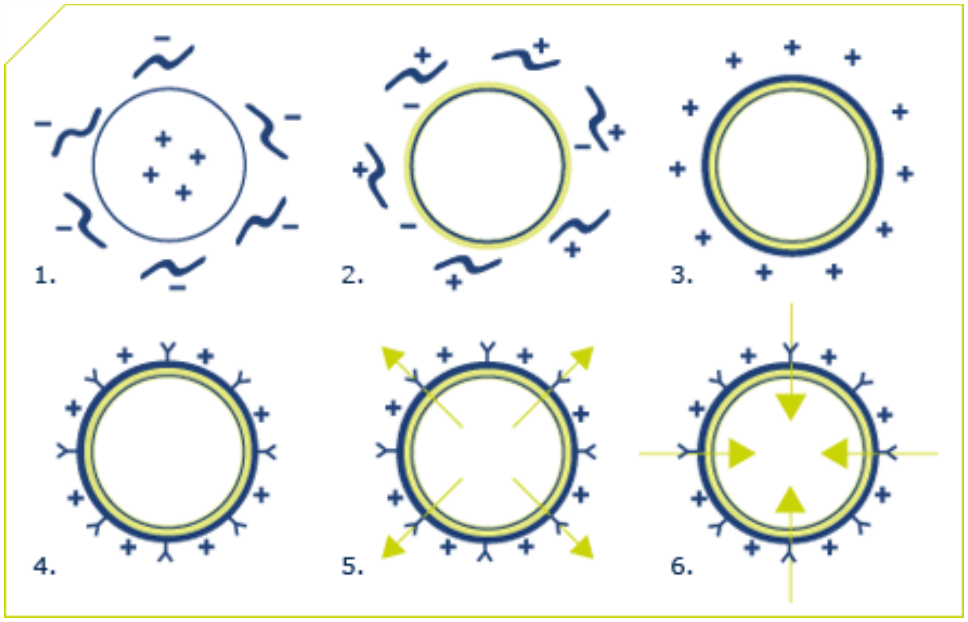

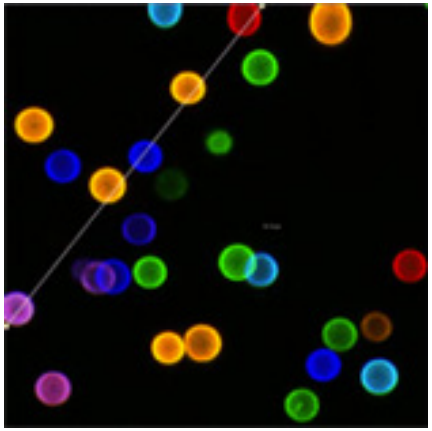

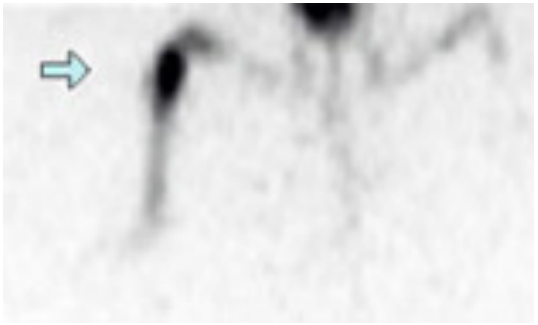

Fluorescent imaging; MRI imaging (e.g., loaded with metal nanoparticles

http://www.capsulation.com; Decher.

Roll-to-roll LBL

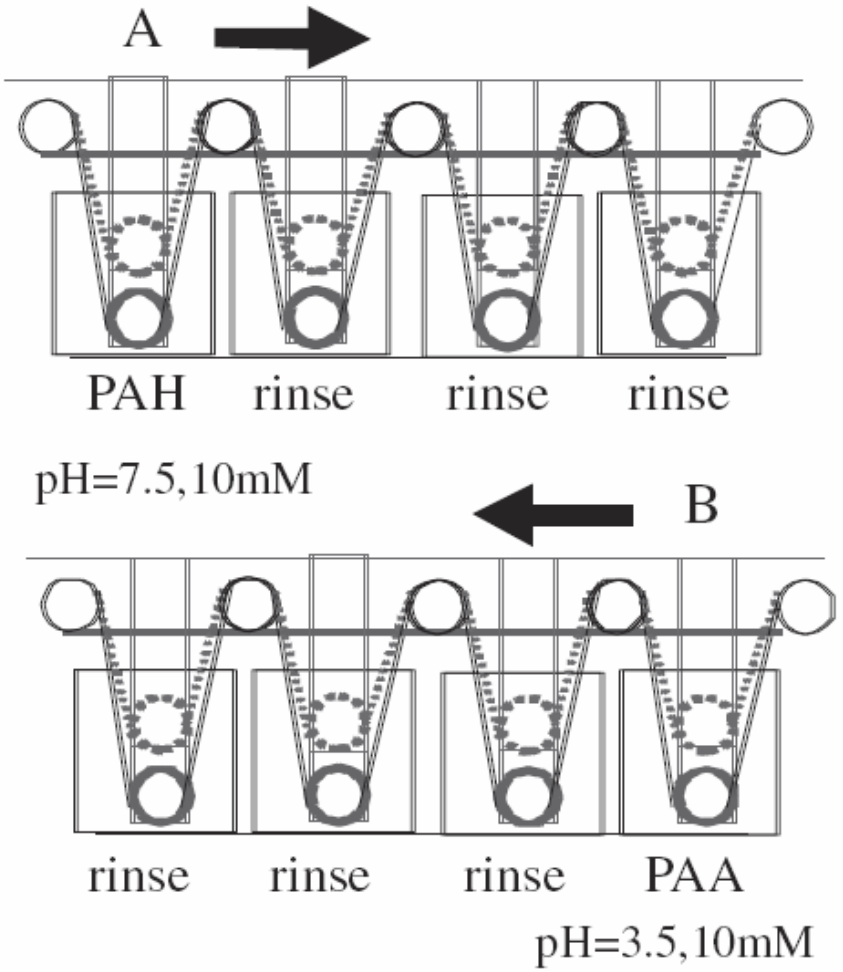

Fig. 1. Schematic of layer-by-layer self-assembly using roll-to-roll process: A is polycation (PAH) and B is polyanion (PAA). Another rinsing process using 18 MΩ Millipore water.

Fujimoto et al., *JJAP* 44(3):126, 2005.

Decher.

The Yasa-sheet, invented by S. Shiratori of Keio University, is equipped with a multilayer film and contains an enzyme (extracted from bamboo) that controls the ethylene concentration and such extends the shelf-life of fruits and vegetables.

The product, sold by PLUSTO (Japan), received the „Excellent Product Award“ of Nikkei in 2001.


Focus
Excelens
CIBA VISION

Assembly of packed particle layers by capillary forces

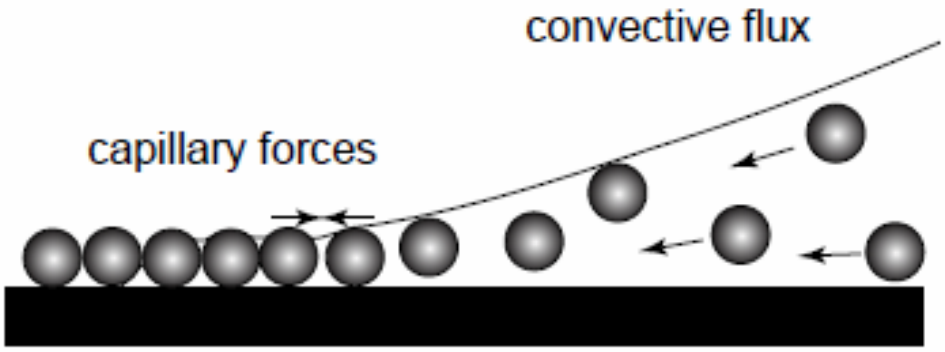

Figure 1.3: Scheme of a drying front with convective flux. Capillary forces are acting between particles at the very front where the liquid film is thinner than the diameter of the particles. Due to increased evaporation of liquid (water) at the drying front a convective water flux is generated which transports particles towards the front.

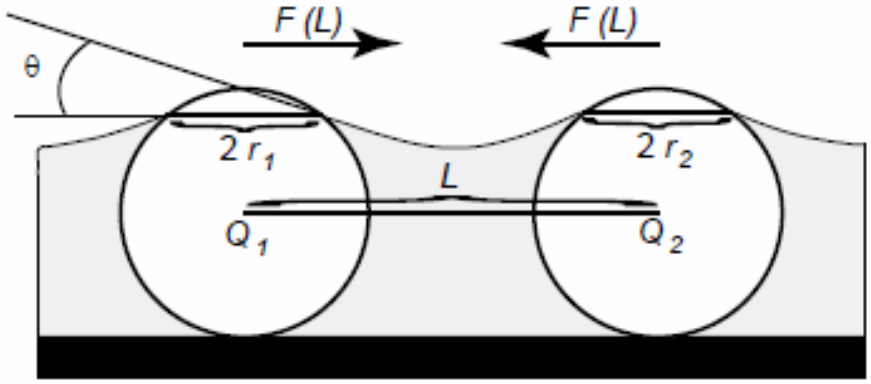

Figure 1.2: Schematic of two particles being attracted through capillary forces. The liquid film is thinner than the diameter of the particles which results in the deformation of the air-liquid interface.

Baettler, PhD. thesis ETH Zurich.

Scaling of capillary forces

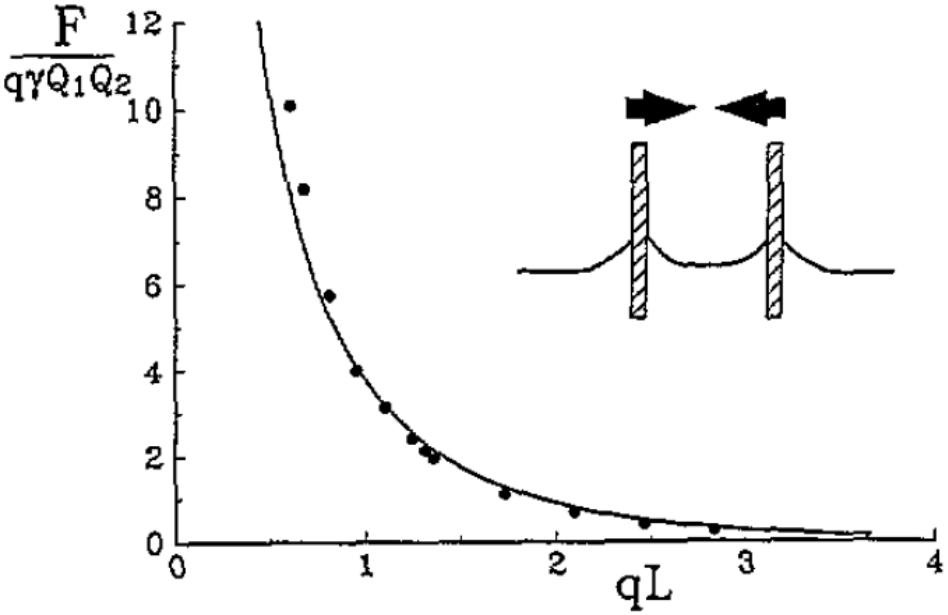

generally scales as 1/ separation

Figure 4. Lateral capillary force, F, versus the distance, L, between two vertical hydrophilic glass capillaries, partially immersed in pure water.

Depends on contact angles, surface energies, difference between particle and fluid densities

deformation. The theory [11, 14–16] provides the following expression for calculating the lateral capillary force between two particles of radii R_1 and R_2 separated by a centre-to-centre distance L

$$F = 2\pi\gamma Q_1 Q_2 q K_1(qL)[1 + O(q^2 R_k^2)] \qquad r_k \ll L \tag{1}$$

where γ is the liquid-fluid interfacial tension, r_1 and r_2 are the radii of the two contact lines and $Q_k = r_k \sin\psi_k$ $(k = 1\,2)$ is the 'capillary charge' of the particle [15, 19];

$$\begin{aligned} q^2 &= \Delta\rho g/\gamma \qquad \text{(in thick films)} \\ q^2 &= (\Delta\rho g - \Pi')/\gamma \qquad \text{(in thin films).} \end{aligned} \tag{2}$$

Here $\Delta\rho$ is the difference between the mass densities of the two fluids and Π' is the derivative of the disjoining pressure with respect to the film thickness; K_1 is the modified Bessel function. The asymptotic form of equation (1) for $qL \ll 1 (q^{-1} = 2.7$ mm for water),

Baettler, PhD. thesis ETH Zurich.

Deposition methods

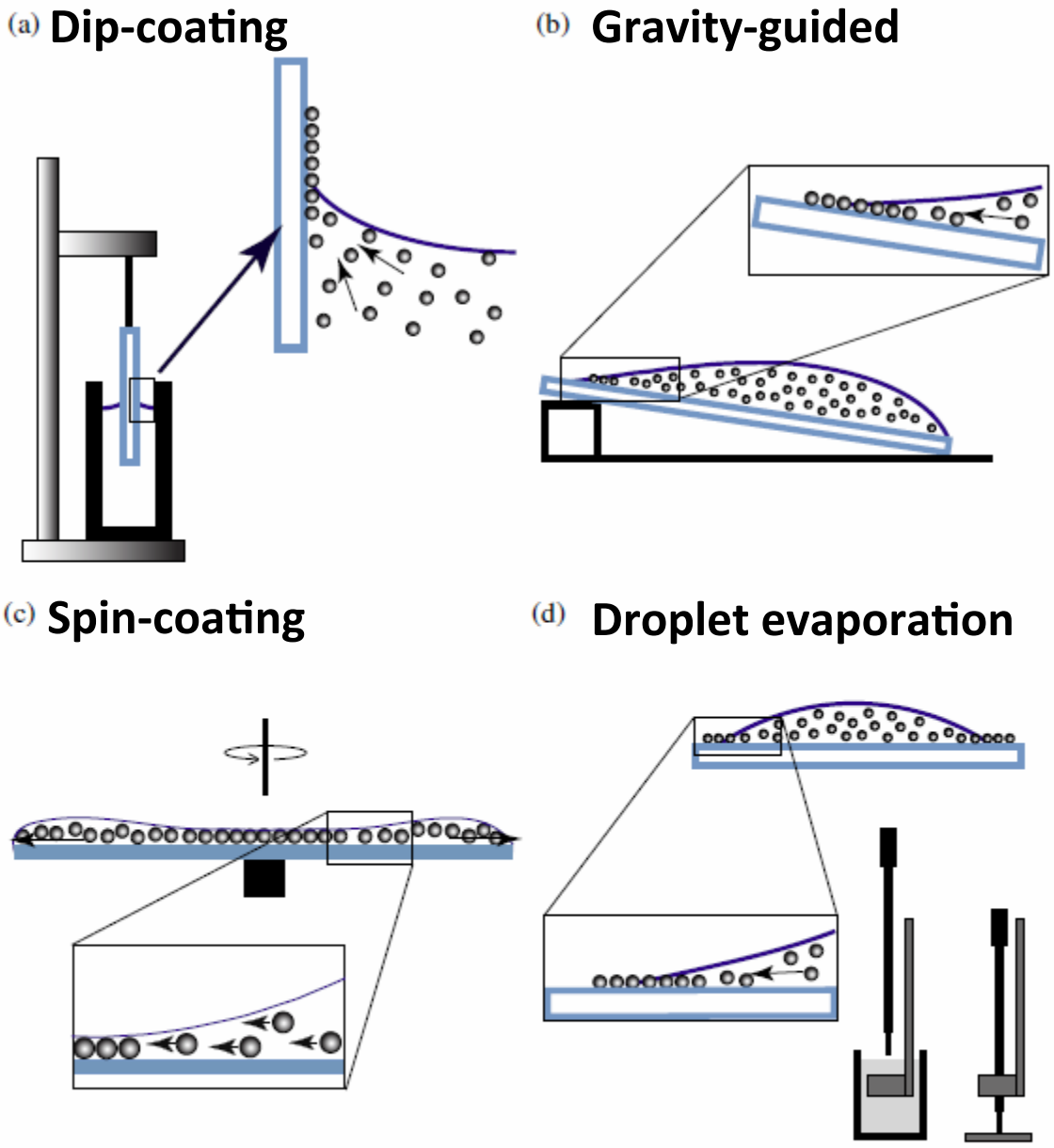

Figure 3.1: Sketches of the four different investigated and used particle self-assembly techniques (not in scale). (a) Vertical particle self-assembly was applied using a computer driven linear motion drive to withdraw a substrate from a particle suspension. Tilted and horizontal assembly were either performed (b) by simply tilting the substrate by approximately 10 % or (c) by spin-coating. (d) Micron-sized drops of suspension were placed on the substrate using a pin-and-ring spotter. The drops were left to dry and formed free-standing particle crystals.

Baettler, PhD. thesis ETH Zurich.

(a) **Higher spin speed**

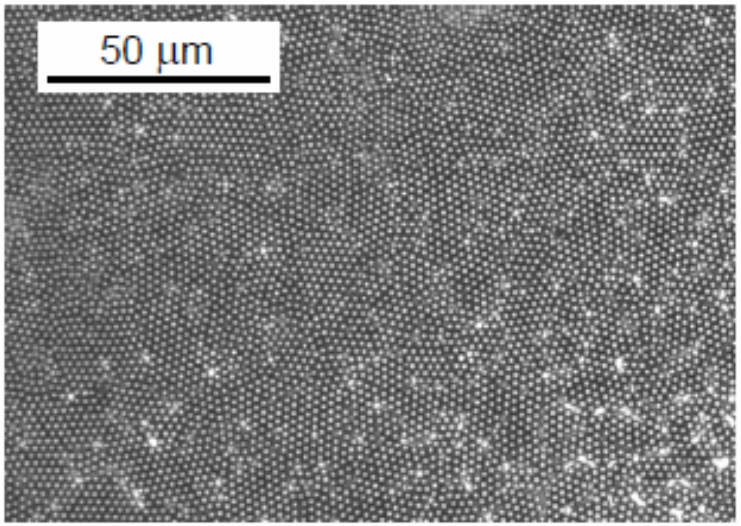

Lower spin speed

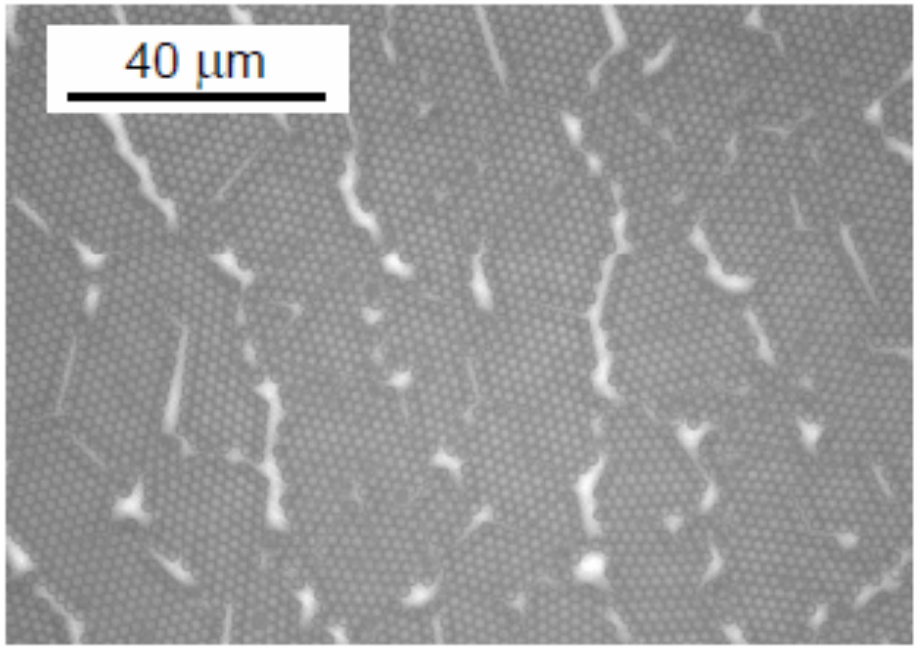

Figure 4.5: Self-assembly of 2.0 μm particles on (a+b) glass slides and (c+d) TiO_2 coated silicon wafers using spin-coating. The images are representative for the assembly of monolayers. The monolayers were packed more exact into hexagonally ordered particle domains on the TiO_2 substrates while the size of the domains was larger in size on glass slides. The samples of the presented SEM images were prepared with spinning speeds of (a) 900, (b) 200, (c) 400 and (d) 100 rpm at different particle concentrations. The spinning-speed influenced the size of the achieved domains in the monolayers. Slower spinning speeds — larger domains.

Baettler, PhD. thesis ETH Zurich.

	33.3 wt%	10 wt%	1 wt%
100 rpm	—	 multilayers	 *monolayers*
300 rpm	 multilayers	 multilayers	 incomplete monolayers
600 rpm	 multilayers	 multilayers	 incomplete monolayers
900 rpm	 multilayers	 *monolayers*	—
1200 rpm	 multilayers	 incomplete monolayers	—
3600 rpm	 multilayers	—	—
6000 rpm	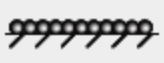 *monolayers*	—	—

Baettler, PhD. thesis ETH Zurich.

Nanosphere lithography

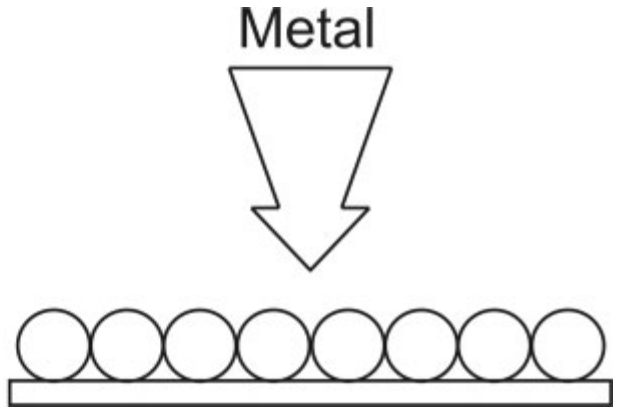

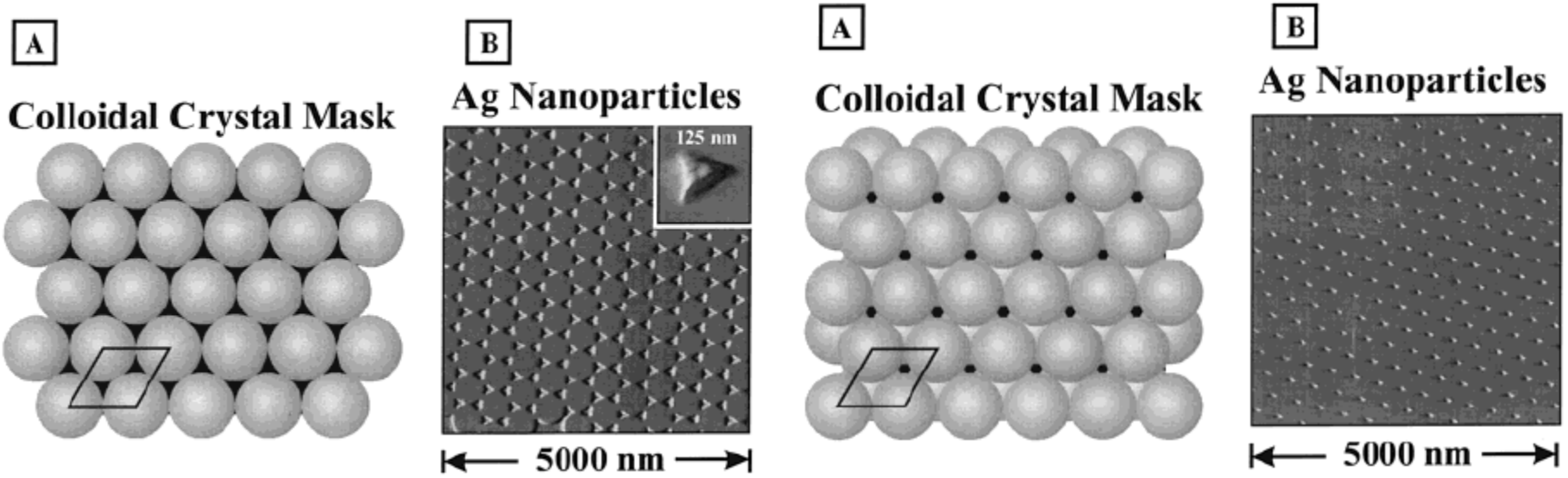

Murray and Barnes, Advanced Materials 19:3771-3782, 2007; van Duyne et al., Northwestern.

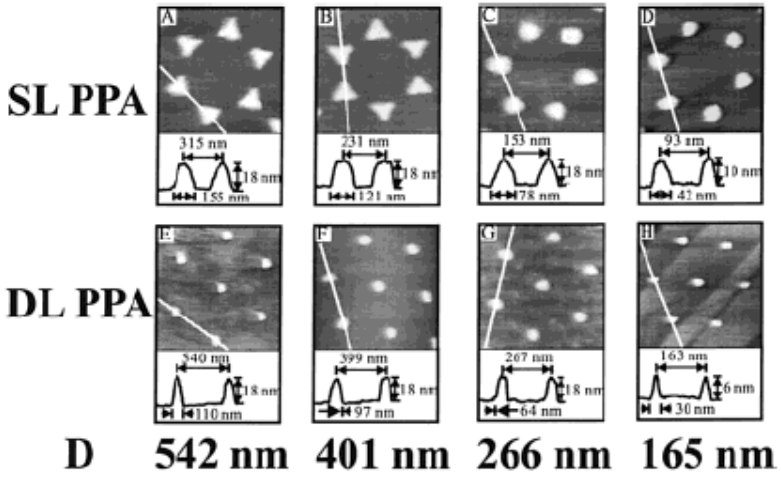

Figure 10. AFM images and line scans of representative Ag nanoparticle arrays on mica substrates. The line scan values reported here have not been deconvoluted for tip broadening effects. (A) 870 nm × 870 nm image, $D = 542$ nm, $d_m = 18$ nm; (B) 610 nm × 610 nm image, $D = 401$ nm, $d_m = 18$ nm; (C) 420 nm × 420 nm image, $D = 264$ nm, $d_m = 18$ nm; (D) 260 nm × 260 nm image, $D = 165$ nm, $d_m = 14$ nm; (E) 1200 nm × 1200 nm image, $D = 542$ nm, $d_m = 18$ nm; (F) 1000 nm × 1000 nm image, $D = 401$ nm, $d_m = 18$ nm; (G) 670 nm × 670 nm image, $D = 264$ nm, $d_m = 18$ nm; (H) 410 nm × 410 nm image, $D = 165$ nm, $d_m = 0.5$ nm.

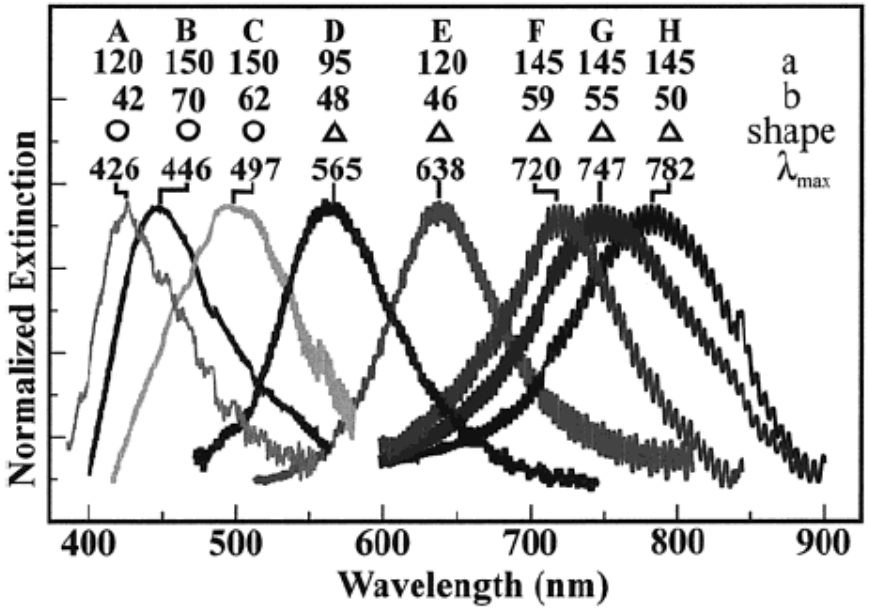

Figure 11. UV−visible extinction spectra of Ag SL PPA on mica substrates. Reported spectra are raw, unfiltered data. The oscillatory signal superimposed on the LSPR spectrum seen in the data is due to interference of the probe beam between the front and back faces of the mica.

Haynes and Van Duyne, *J. Physical Chemistry B* 105:5599:5611, 2001.

Templated sphere packing

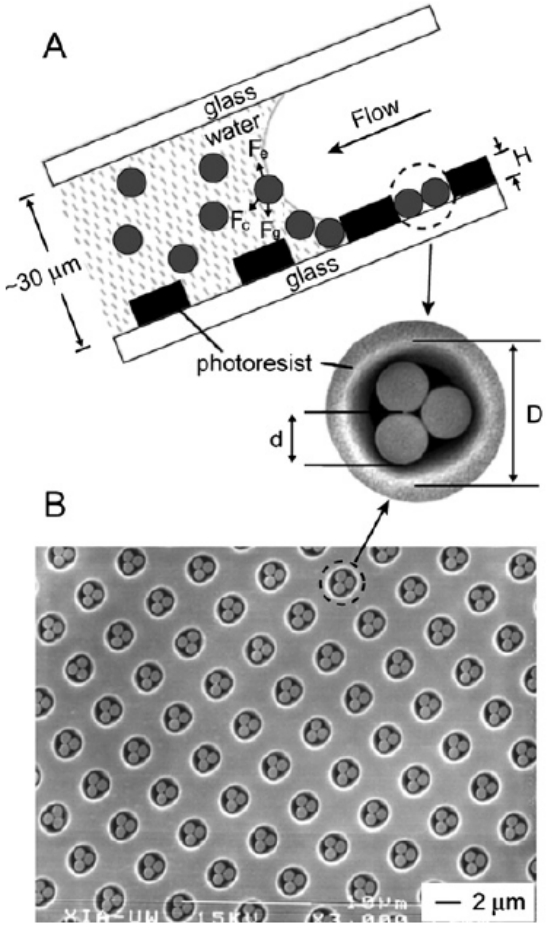

Fig. 1 (A) A schematic illustrating the fluidic cell used in a TASA process as discussed in this highlight article. The template hole depth is indicated by H, the diameter of the template is D, and the diameter of the colloidal spheres is d. The possible forces that may be exerted on a colloidal sphere next to the rear edge of the liquid slug are the capillary force (F_c), gravitational force (F_g) and electrostatic force (F_e) and are illustrated above. (B) SEM image of an example of TASA where a two-dimensional array of trimers was formed from 0.9 μm PS beads.

Rycenga et al., *Soft Matter* 5:1129-1136, 2009.

Geometric shape of the template	Structure of the cluster	Requirements
D	d	D/d = 1.00-2.00
		D/d = 2.00-2.15
		D/d = 2.15-2.41
		D/d = 2.41-2.70
		D/d = 2.70-3.00
		D/d = 3.00-3.30
a		a = 2d
L W		L = 4d W = d
		d < w < 2d
L		L = 2.73d
D D'		D = 3d D' = d

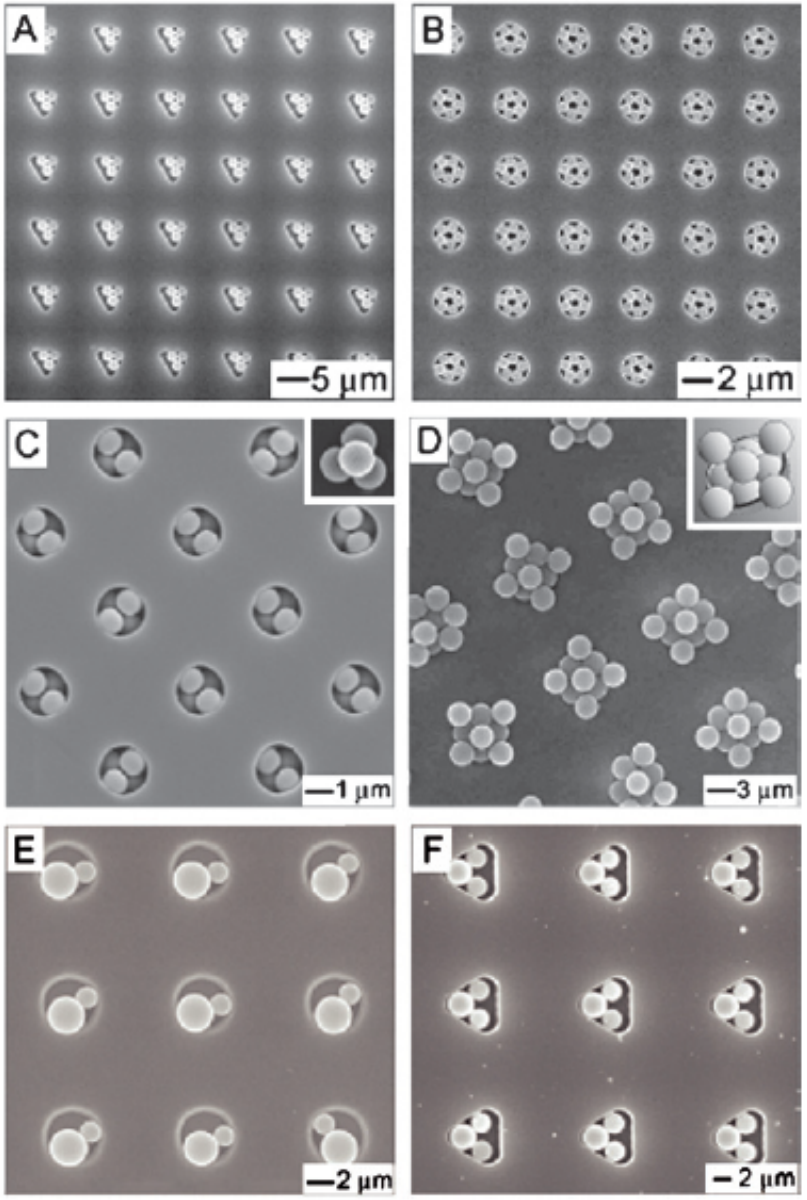

Rycenga et al., *Soft Matter* 5:1129-1136, 2009.

3D colloidal crystals and superlattices

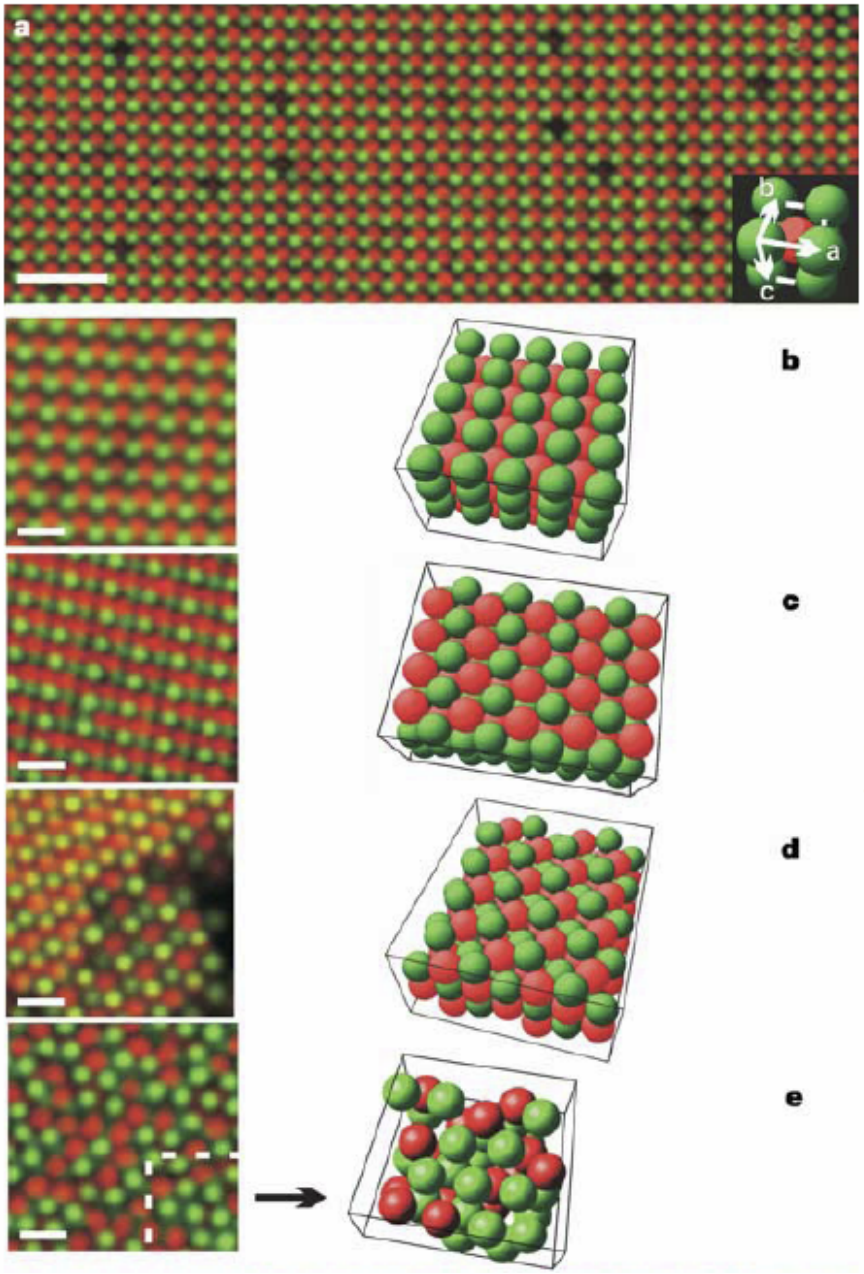

Figure 1 | CsCl-type binary crystals. **a–e**, Positive (red, radius 1.08 μm) and negative (green, 0.99 μm) PMMA-spheres. **a**, Confocal micrograph of a large (100) plane (scale bar, 10 μm). Inset, the cubic CsCl-type unit cell. **b–d**, Close-up of the (100), (110) and (111) planes plus corresponding models. **e**, 'Solid solution'. The stacking of the hexagonal layers is visible in the box with rendered coordinates. The model spheres have a smaller radius for clarity. **f**, CsCl (100) and **g**, (110) planes with positive PMMA (green, 0.52 μm) and negative silica (red, 0.58 μm) particles. Scale bars in **b–g**, 4 μm. All particles were dispersed in TBAB-containing CHB-decalin.

Nanoparticle superlattices

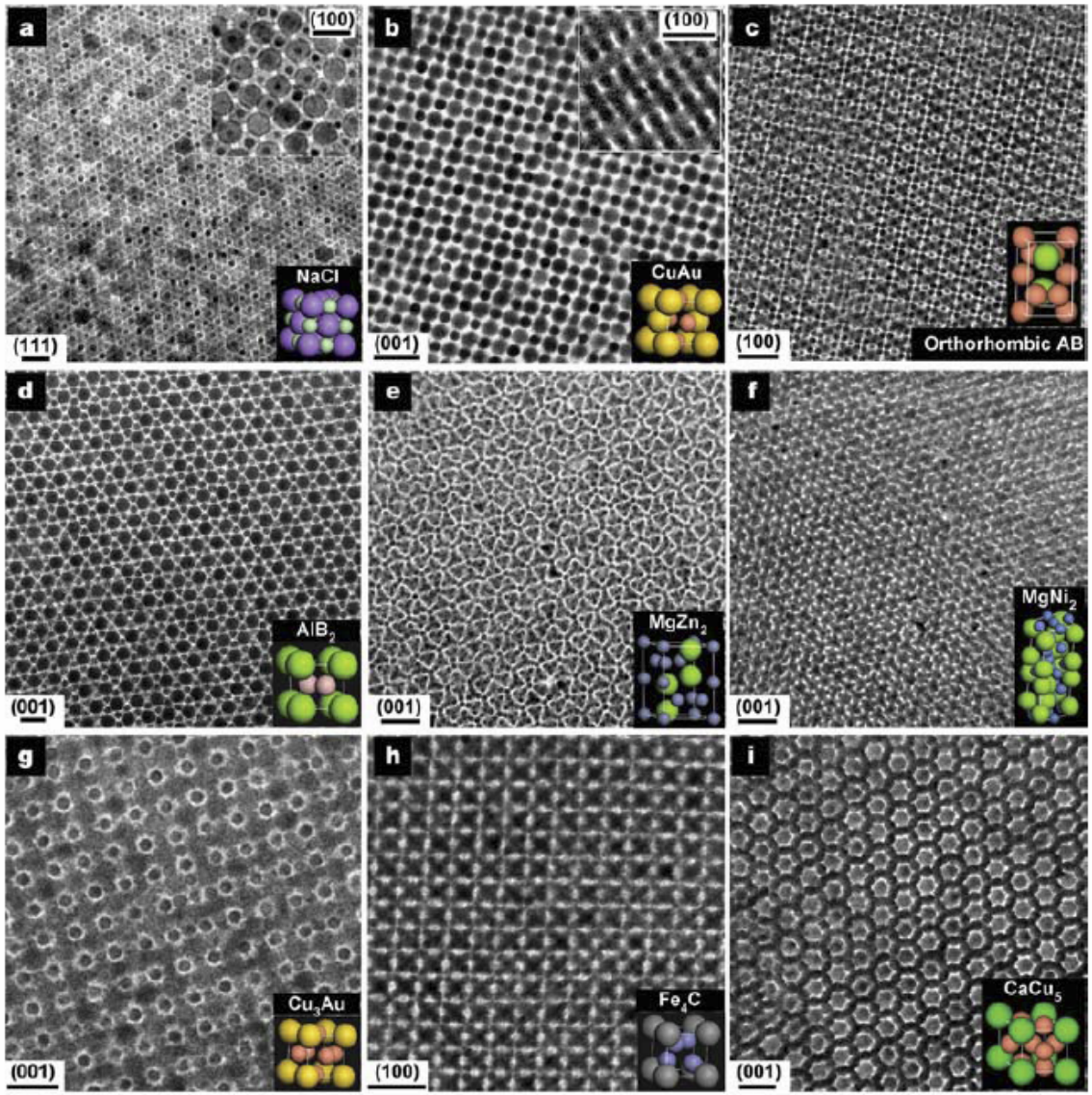

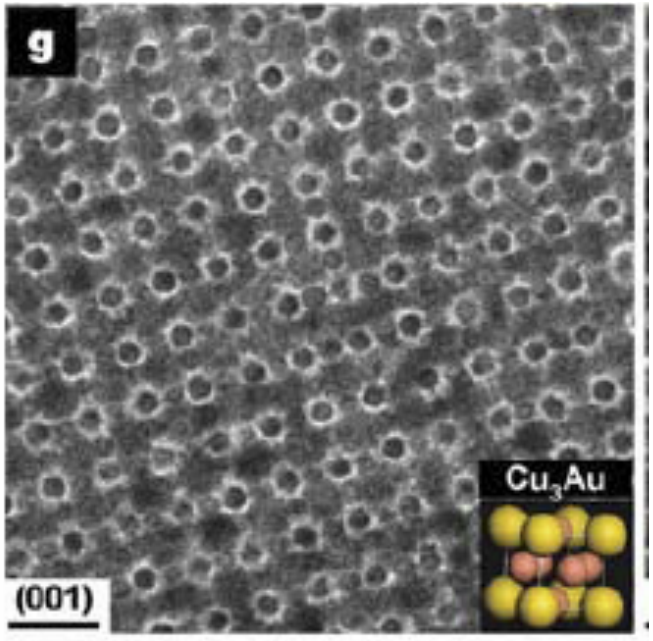

Figure 1 | TEM images of the characteristic projections of the binary superlattices, self-assembled from different nanoparticles, and modelled unit cells of the corresponding three-dimensional structures. The superlattices are assembled from **a**, 13.4 nm γ-Fe_2O_3 and 5.0 nm Au; **b**, 7.6 nm PbSe and 5.0 nm Au; **c**, 6.2 nm PbSe and 3.0 nm Pd; **d**, 6.7 nm PbS and 3.0 nm Pd; **e**, 6.2 nm PbSe and 3.0 nm Pd; **f**, 5.8 nm PbSe and 3.0 nm Pd; **g**, 7.2 nm PbSe and 4.2 nm Ag; **h**, 6.2 nm PbSe and 3.0 nm Pd; **i**, 7.2 nm PbSe and 5.0 nm Au; **j**, 5.8 nm PbSe and 3.0 nm Pd; **k**, 7.2 nm PbSe and 4.2 nm Ag; and **l**, 6.2 nm PbSe and 3.0 nm Pd nanoparticles. Scale bars: **a–c**, **e**, **f**, **i–l**, 20 nm; **d**, **g**, **h**, 10 nm. The lattice projection is labelled in each panel above the scale bar. The modelled projections of the binary superlattices are shown in Supplementary Fig. 4.

Shevchenko et al.

Self-assembled nanoparticle rings

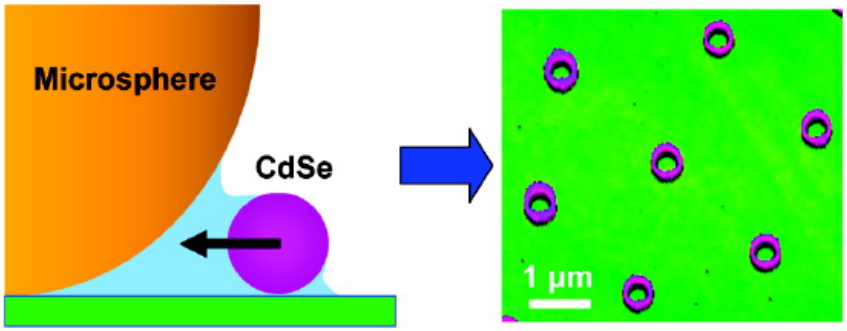

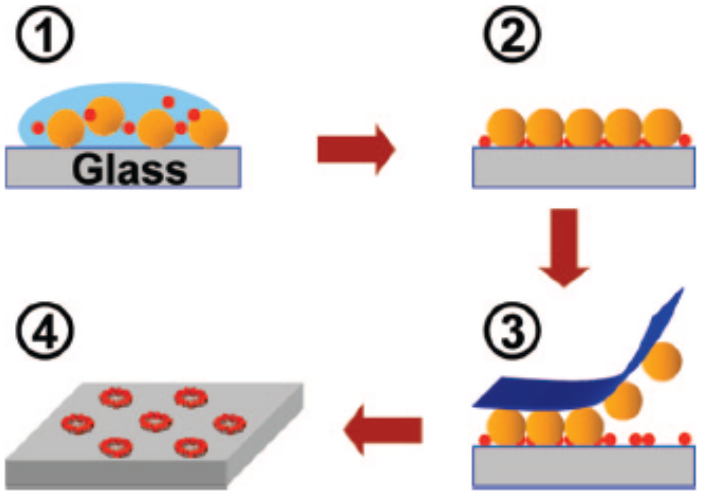

Figure 1. Schematic diagram of the evaporation templating procedure employed for forming CdSe nanorings (red particles) on planar substrates using microsphere templates (orange particles). Note that the drawing is not to scale.

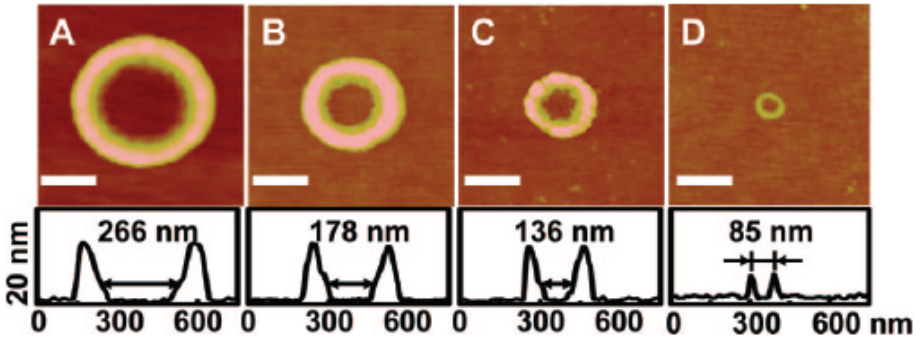

Figure 6. AFM topographical images and the corresponding line profiles from single CdSe nanorings formed with polystyrene spheres having diameters of (A) 2 μm, (B) 1 μm, (C) 600 nm, and (D) 200 nm. All scale bars are 200 nm long. The evaporative templating process was carried out at a CdSe concentration of 2×10^{13} QDs/mL under all conditions. The microsphere concentrations in the initial aqueous solutions were (A) 1×10^{10} spheres/mL, (B) 2×10^{10} spheres/mL, (C) 8×10^{10} spheres/mL, and (D) 3×10^{11} spheres/mL, respectively.

Chen et al., *ACS Nano* 3(1):173-180, 2009.

Geometric constraints and force balance

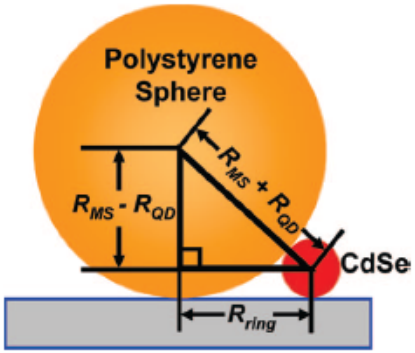

Figure 8. Schematic diagram of the hard sphere contact model employed for calculating the contact radius of the CdSe nanorings. Note that the drawing is not to scale.

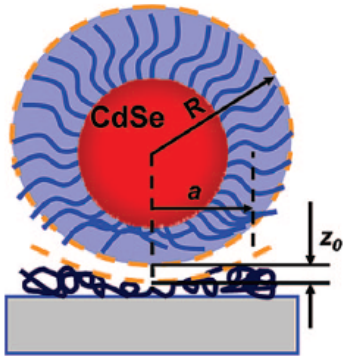

Figure 11. Schematic diagram of a 16-MHA capped CdSe quantum dot in contact with a PVP-modified glass substrate. Note that the drawing is not to scale.

- Surfactant/SAM gets in the way

- Capillary forces (attraction)
- Adhesion forces (attraction)
- Electrostatic forces (repulsion)

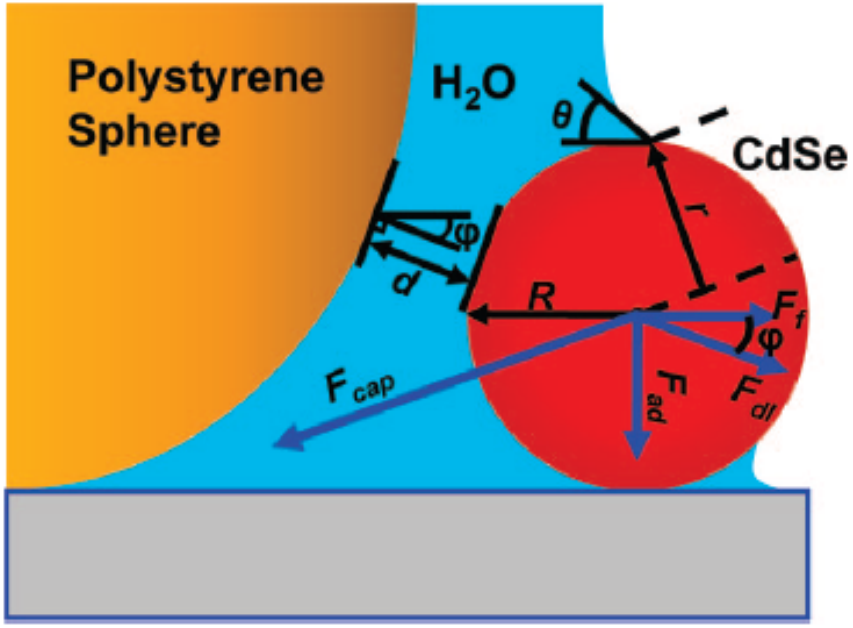

Chen et al., *ACS Nano* 3(1):173-180, 2009.